Assessment of gas-particle flow models for pseudo-2D fluidized bed applications

Cesar M. Venier, Santiago Marquez Damian & Norberto M. Nigro

Published online: 26 Jan 2018.

Submit your article to this journal ⬈

View related articles ⬈

View Crossmark data ⬈

Taylor & Francis
Taylor & Francis Group

Check for updates

Assessment of gas-particle flow models for pseudo-2D fluidized bed applications

Cesar M. Venier[a,b] , Santiago Marquez Damian[a,c], and Norberto M. Nigro[a,d]

[a]Research Center for Computational Methods (CIMEC), CONICET, Santa Fe, Argentina; [b]Facultad de Ciencias Exáctas, Ingeniería y Agrimensura, Universidad Nacional de Rosario, Santa Fe, Argentina; [c]Facultad Regional Santa Fe, Universidad Tecnológica Nacional, Santa Fe, Argentina; [d]Facultad de Ingeniería y Ciencias Hídricas, Universidad Nacional del Litoral, Santa Fe, Argentina

ABSTRACT

The aim of this work is to provide more insight into the general modeling criteria for simulating pseudo-2D bubbling fluidized beds. For this purpose, two experimental-based problems are studied. First, a fluidized bed with a high-speed central jet problem is analyzed. A qualitative study of the first bubble indicates that the bubble shape prediction is highly sensitive to the frictional model adopted. The most accurate results in terms of bubble shape and detachment time are given by a frictional model that relates the strain-rate fluctuations with the granular temperature. Second, a uniformly fluidized bed problem in bubbling regime is considered. For this case, the drag models and boundary conditions for the particulate phase are investigated. Time-averaged solid phase velocity profiles are compared with the results of the literature where it is found that no-slip conditions (or partial slip with a high specularity coefficient) are more appropriate than slip conditions at the walls for these regimes. Regarding the drag force, although none of the models presented could match the experimental velocity predictions for low gas velocities at the lower region of the bed, the Di Felice model produces the most accurate results for the whole range of regimes considered.

Introduction

Granular materials have diverse industrial applications. Many of these require an agitated regime to favor the contact with a fluid phase and, therefore, increase the mass and energy transfer rates. Fluidized bed arrangements have these features. They consist of a large container in which a bed of particles are fluidized by means of an air flow that is blown from below. Different fluidized bed regimes may be obtained by modifying the air inlet flow, the particles size, the solid material and the container dimensions. Due to its multiple applications (e.g., catalytic cracking, grain drying, ethanol polymerization, coal gasification) and the various regimes that may be obtained, the design of fluidized bed systems require a proper understanding of the multiphase flow behavior.

For this purpose, pseudo-2D fluidized bed arrangements are commonly used for lab-scale experiments since it allows a direct observation of the gas-particles hydrodynamics. However, experimental approaches are usually costly and involve a well-trained laboratory staff. In this context, the computational fluid dynamics techniques come as a nonexpensive approach to address fluidized bed problems and to complement the experimental data. The Eulerian two-fluid model (TFM) is one of the main approaches that has proven to be successful in predicting the hydrodynamic behavior of granular flows in fluidized beds (Ding and Gidaspow, 1990; Yuu et al., 2001; Taghipour et al., 2005; Koksal and Hamdullahpur, 2005; Mazzei, 2008; Parmentier et al., 2008; Wang et al., 2008). This model is based on treating both phases as interpenetrating continua which leads to a system of averaged Navier–Stokes equations (Ishii, 1975; Drew, 1982; Enwald et al., 1996). These equations require closure models to handle the solid particles interaction effect on the solid stress tensor and the momentum exchange between phases.

In the early years, the solid stress tensor was modeled by considering the granular material as a fluid with a constant viscosity and a particles pressure function added to the normal component of the stress tensor, which grows as the particles concentration increases (Bouillard et al., 1989; Lyczkowski et al., 1993). With the development of the kinetic theory of granular flow (KTGF) (Lun et al., 1984; Gidaspow, 1994), investigations on particulate flow modeling gained more attention from the community. In contrast with previous theories, the KTGF, which derives from the dense gas theory of Chapman and Cowling (1970), has a deeper phenomenological basis. This theory considers the particles as uniform spheres, and the collisions between them are considered instantaneous. The impact of these interactions on the rheological parameters are then related to the random motion of particles. This random motion is quantified by introducing the granular temperature concept which evolves following a granular energy balance equation.

It also became clear that, when particles are in higher concentrations, the collisions are no longer instantaneous leading to rubbing and frictional effects. In such cases, the solid phase shear stress tensor is often modeled by the frictional theory (Schaeffer, 1987; Johnson and Jackson, 1987) which is mostly based on the critical state theory of soil mechanics (Atkinson and Bransby, 1977). In particular, the Syamlal model (Syamlal et al., 1993) and the Johnson–Jackson model (Johnson and Jackson, 1987) for the particles pressure are arguably the most used in the literature (Passalacqua and Marmo, 2009; Patil et al., 2005a,b). The first one considers a solid pressure that scales up very quickly for solid volume fractions above a minimal limit at which friction effects occur, while the second one adopts an additive approach with the kinetic effects and takes into account the maximum packing. In the last years, a model based on the work of Srivastava and Sundaresan (2003) has become widely used in the literature (Benyahia, 2008; Passalacqua and Marmo, 2009). From a physical point of view, the model has a deeper phenomenological basis, since it takes the additive approach of Johnson and Jackson along with a modified shear stress model to account for the strain rate fluctuation for quasi-static flow based on the work of Savage (1998).

For fluidized bed applications, the drag is usually the only interfacial force considered and many correlations for the drag force coefficient can be found in the literature. The Wen–Yu model (Wen and Yu, 1966) is applicable for low particles concentration and it is based on the free falling velocity of a particle extended to multiple particles in liquid–solid suspensions based on the experimental work of Richardson and Zaki (1954). However, the Ergun model (Ergun, 1952) is developed for packed beds and properly describes the drag forces in high particles concentrations. Later on, Gidaspow (1994) proposed a drag model that consist on a switching technique between the Wen–Yu model (for $\alpha_s \leq 0.2$) and the Ergun model (Ergun, 1952) (for $\alpha_s > 0.2$). Other models, like the Syamlal–O'Brien model (Syamlal, 1987), the Gibilaro model (Gibilaro et al., 1985) and the Arastoopour model (Arastoopour et al., 1990) have extended the concept based on the terminal velocity of Wen and Yu for more general cases avoiding the switching technique of the Gidaspow model. Further on, Di Felice (1994) extended the approach of Wen and Yu to contemplate multiple regimes by introducing a voidage function dependent of the particles Reynolds number. While the impact of each model have been studied for fluidized bed problems over the years, there is no common agreement on which is the most proper to replicate the experimental results for different bubbling regimes (Esmaili and Mahinpey, 2011; Du et al., 2006; Loha et al., 2012). Moreover, the relative performance of such models in pseudo-2D simulations is a topic barely discussed in the literature.

The correct choice for the particulate phase wall boundary conditions in fluidized bed applications is also a common topic of discussion (Hui et al., 1984; Johnson and Jackson, 1987; Jenkins and Richman, 1986; Benyahia et al., 2005; Konan et al., 2006; Schneiderbauer et al., 2012; Soleimani et al., 2015; Fede et al., 2016). Among them, the Johnson–Jackson boundary conditions (Johnson and Jackson, 1987) for the solid velocity and granular energy are usually associated with rough walls and introduce the wall restitution and the specularity coefficient as input parameters. This last parameter somehow measures the roughness of the wall affecting the amount of sliding that the particles experience. Benyahia et al. (2005) studied

various conditions for the solid phase for a circulating gas–solid system and concluded that low values of the specularity coefficient (even fully slip conditions) are proper to represent the patterns of the experimental results. However, for bubbling fluidized conditions, Fede et al. (2016) observed that the simulations performed with a fully nonslip boundary conditions for the solid phase at the walls have a satisfactory agreement with the experimental data. Moreover, the direct use of the Johnson–Jackson model involves an estimation of the specularity coefficient which, in turn, is a nonmeasurable parameter. To avoid this issue, Li and Benyahia (2012) proposed a definition of the specularity as a function of other flow variables. In the same spirit, Schneiderbauer et al. (2012) proposed a different theory that combines sliding and nonsliding conditions introducing the wall friction factor and the tangential restitution coefficient.

In this work, a predeveloped conservative gas-particle flow solver with kinetic-frictional theory closure (Venier et al., 2016) is used to explore various modeling aspects for two typical pseudo-2D fluidized bed problems based on the experimental setups of Kuipers et al. (1991) and Laverman et al. (2008). Regarding the mentioned models, as far as the authors knowledge, there is no absolute agreement from the community about which set is the most proper to be used for simulating bubbling fluidized bed systems. Therefore, a purpose of the present work is to examine the results given by these models in terms of time-averaged solid velocity and volume fraction field and provide more insight about optimal pseudo-2D simulations setup.

The following sections are presented in the following order: "Eulerian two-fluid model" section presents the TFM with the corresponding kinetic and frictional closure theories. In "Results" the presented models are explored for two standard fluidized bed problems and the simulations are compared with the experimental results of the literature. Finally, in "Conclusion" the main conclusions of this work are outlined.

Eulerian two-fluid model

The TFM considers both phases as interpenetrating continuous media, where the mass and momentum conservation equations are obtained by averaging techniques (Enwald et al., 1996). This procedure introduces the volumetric phase fraction field α_i that verifies: $\alpha_s + \alpha_g = 1$. Here s represents the particulate phase and g represents the gas phase.

Both phase continuity and momentum equations are presented below:

$$\frac{\partial}{\partial t}(\rho_s \alpha_s) + \nabla \cdot p(\rho_s \alpha_s \mathbf{u}_s) = 0 \qquad (1)$$

$$\frac{\partial}{\partial t}(\rho_g \alpha_g) + \nabla \cdot p(\rho_g \alpha_g \mathbf{u}_g) = 0 \qquad (2)$$

$$\frac{\partial}{\partial t}(\rho_s \alpha_s \mathbf{u}_s) + \nabla \cdot (\rho_s \alpha_s \mathbf{u}_s \mathbf{u}_s) = $$
$$- \alpha_s \nabla p - \nabla p_s + \nabla \cdot (\alpha_s \tau_s) + \rho_s \alpha_s \mathbf{g} + K_{sg}(\mathbf{u}_g - \mathbf{u}_s) \qquad (3)$$

$$\frac{\partial}{\partial t}(\rho_g \alpha_g \mathbf{u}_g) + \nabla \cdot (\rho_g \alpha_g \mathbf{u}_g \mathbf{u}_g) = $$
$$- \alpha_g \nabla p + \nabla \cdot (\alpha_g \tau_g) + \rho_g \alpha_g \mathbf{g} + K_{sg}(\mathbf{u}_s - \mathbf{u}_g) \qquad (4)$$

where the shear stress tensors are modeled as:

$$\tau_s = \mu_s \big[\nabla \mathbf{u}_s + \nabla \mathbf{u}_s^T\big] + \left(\lambda_s - \frac{2}{3}\mu_s\right)(\nabla \cdot \mathbf{u}_s)\mathbf{I} \quad (5)$$

$$\tau_g = \mu_g \big[\nabla \mathbf{u}_g + \nabla \mathbf{u}_g^T\big] - \frac{2}{3}\mu_g(\nabla \cdot \mathbf{u}_g)\mathbf{I} \quad (6)$$

Here $\mathbf{u}_i$ is the phase velocity, $\mathbf{g}$ the gravitational acceleration, K_{sg} the drag coefficient, ρ_i the phase density, μ_i the phase dynamic viscosity, p the shared pressure, p_s the particle pressure field, and λ_i the phase bulk viscosity.

Drag models

In the present multiphase model, the exchange of momentum between phases is given by the drag force exclusively. Other forces, such as the lift and virtual mass, are neglected. Many correlations for the drag coefficient have been developed over the years. In particular, the Ergun equation (Ergun, 1952) is commonly applied to predict the pressure drop in packed beds of particles. However, for fluidized conditions, this simple formula is no longer applicable. The first attempts to establish a general drag law for more diluted conditions were done by Richardson and Zaki (1954). They investigated the sedimentation of spherical particles in a liquid–solid suspension to obtain an expression for the

relative velocity as a function of the voidage fraction. The results of their experiments have been extensively used to develop several correlations for the drag coefficient. In particular, the Wen–Yu drag model (Wen and Yu, 1966) uses this information and extended the drag force applied on a single particle to a system of particles. This correlation relies on the hypothesis that the flow is dominated by viscous forces. In the same spirit, Syamlal (1987) proposed a model extending the single-particle approach to multi-particles systems, but introducing a relative velocity correlation which is function of the particle Reynolds number and the voidage fraction following the experimental results of Richardson and Zaki. This model considers that the Archimedes number (relating the gravitational and viscous forces) is the same for a single particle and for a system of particles. However, Gidaspow (1994) proposed a switching technique at $\alpha_g = 0.8$ between the Wen–Yu coefficient for diluted regimes and the Ergun correlation for packed conditions, to contemplate the various states of particle concentrations. The coefficient obtained by this approach has the disadvantage of being discontinuous at the point of switching. The Gibilaro model (Gibilaro et al., 1985) is another example of a drag law designed to extend the applicability of a fixed bed correlation (i.e., the Ergun equation). In fact, this predictive expression can be seen as a modified version of the Ergun model with a different friction factor that only depends on the particles Reynolds number and adjusted to match the experimental data. Later on, Arastoopour et al. (1990) made slight modifications on the expression of Gibilaro in how the drag force is affected by the void fraction. More recently, Di Felice (1994) followed the general structure of the Wen–Yu model modifying the expression to account for intermediate flow regimes with a function based on a data fitting of experimental results.

The aforementioned models are among the most frequently used for fluidization conditions in the literature. Figure 1 shows the drag coefficient as a function of the particles concentration, maintaining the rest of the parameters fixed. For this graphic, typical bubbling fluidization conditions are considered with densities of $\rho_s = 2500$ and $\rho_g = 1.2$ kg/m^3 for the solid phase and the gas phase
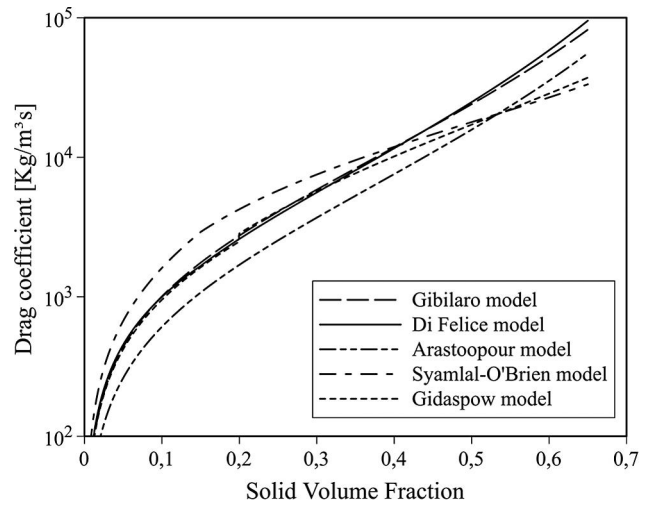

Figure 1. Drag coefficient K_{sg} as function of the particles concentration for each model at bubbling fluidization conditions.

respectively, a particles uniform diameter of $d_p = 280 \times 10^{-3}$ mm and a constant relative velocity fixed at $|\mathbf{u}_s - \mathbf{u}_g| = 1$ m/s. Although this last parameter will hardly be constant over time and space, it helps to provide an estimation of the relative behavior of the drag models considered. Most of the models predict similar results, however it can be observed that the Syamlal–O'Brien model predicts higher values of the drag force, while the Arastoopour model predicts the lowest drag for low to intermediate particles concentration for the given problem conditions.

Gibilaro model (Gibilaro et al., 1985)

$$K_{sg} = \left[\frac{17.3}{Re_p} + 0.336\right] \frac{\alpha_s \rho_g |\mathbf{u}_g - \mathbf{u}_s|}{d_p} \alpha_g^{-1.8} \quad (7)$$

$$Re_p = \frac{\alpha_g \rho_g d_p |\mathbf{u}_g - \mathbf{u}_s|}{2\mu_g} \quad (8)$$

Gidaspow model (Gidaspow, 1994)

$$K_{sg} = \begin{cases} 150\frac{\mu_g \alpha_s^2}{d_p^2 \alpha_g^2} + 1.75\frac{\rho_g \alpha_s}{d_p \alpha_g}|\mathbf{u}_g - \mathbf{u}_s| & \alpha_s > 0.2 \\ 0.75\frac{C_d \alpha_s \rho_g |\mathbf{u}_g - \mathbf{u}_s|}{d_p} \alpha_g^{-2.65} & \alpha_s \leq 0.2 \end{cases}$$
$$(9)$$

$$C_d = \begin{cases} \frac{24}{Re_p}(1 + 0.15 Re_p^{0.687}) & Re_p < 1000 \\ 0.44 & Re_p \geq 1000 \end{cases} \quad (10)$$

$$Re_p = \frac{\rho_g d_p |\mathbf{u}_g - \mathbf{u}_s|}{\mu_g} \tag{11}$$

Syamlal–O'Brien model (Syamlal, 1987)

$$K_{sg} = 0.75 \frac{C_e \alpha_s \alpha_g \rho_g |\mathbf{u}_g - \mathbf{u}_s|}{d_p v_{rs}^2} \tag{12}$$

$$v_{rs} = 0.5 \Big[A - 0.06 Re_p + \sqrt{(0.06 Re_p)^2 + 0.12 Re_p(2B - A) + A^2} \Big] \tag{13}$$

$$C_e = \left[0.63 + \frac{4.8}{\sqrt{\frac{Re_p}{v_{rs}}}} \right], A = \alpha_g^{4.14}, \tag{14}$$

$$B = \begin{cases} C_2 \alpha_g^{1.28}, \alpha_g \leq 0.85 \\ \alpha_g^{C_1}, \alpha_g > 0.85 \end{cases}$$

where C_1 and C_2 are usually set at 2.65 and 0.8, respectively.

Arastoopour model (Arastoopour et al., 1990)

$$K_{sg} = \left[\frac{17.3}{Re_p} + 0.336 \right] \frac{\alpha_s \rho_g |\mathbf{u}_g - \mathbf{u}_s|}{d_p} \alpha_g^{-2.8} \tag{15}$$

Di Felice model (Di Felice, 1994)

$$K_{sg} = 0.75 \frac{C_e \alpha_s \rho_g |\mathbf{u}_g - \mathbf{u}_s|}{d_p} \alpha_g^{-\chi} \tag{16}$$

$$\chi = P - Q \exp\left[\frac{-(1.5 - log(Re_p))^2}{2} \right] \tag{17}$$

where P and Q are usually set at 3.7 and 0.65 respectively.

Kinetic-collisional particles interaction

The mathematical closure of the TFM is given by the frictional and kinetic-collisional theories through the definition of the rheological parameters of the granular phase. This relies on the various states of particles concentration. The kinetic-collisional regime is modeled by the KTGF (Lun et al., 1984; Gidaspow, 1994), which occurs at low concentration where only binary collisions between particles are possible. This theory is based on the kinetic theory for dense gases (Chapman and Cowling, 1970). The solid phase viscosity and

particles pressure are modeled through the granular temperature θ. This field follows an energy balance equation given by:

$$\frac{3}{2}\left[\frac{\partial}{\partial t}(\rho_s \alpha_s \theta) + \nabla \cdot (\rho_s \alpha_s \mathbf{u}_s \theta) \right] = \tag{18}$$
$$(\tau_s - p_s \mathbf{I}) : \nabla \mathbf{u}_s + \nabla \cdot p(\kappa_s \nabla \theta) - \gamma_s + J_v + J_s$$

where γ_s the dissipation of granular energy due to collisions, κ_s is the conductivity of granular temperature, J_s the granular energy production due to slip between phases, and J_v the dissipation due to viscous damping.

Most of the remaining parameters are modeled according to the works of Gidaspow (1994), Lun et al. (1984), and Sinclair and Jackson (1989):

$$p_{s,ktgf} = \rho_s \alpha_s \theta + 2\rho_s \alpha_s^2 g_0(1 + e)\theta \tag{19}$$

$$\lambda_s = \frac{4}{3}\rho_s \alpha_s^2 d_p g_0(1 + e)\left(\frac{\theta}{\pi} \right)^{1/2} \tag{20}$$

$$\gamma_s = 3(1 - e^2)\alpha_s^2 \rho_s g_0 \theta \left[\frac{4}{d_p}\sqrt{\frac{\theta}{\pi}} - \nabla \cdot p\mathbf{u}_s \right] \tag{21}$$

$$J_v = -3K_{sg}\theta \tag{22}$$

$$J_s = K_{sg}\left[3\theta - \frac{K_{sg}d_p(\mathbf{u}_g - \mathbf{u}_s)^2}{4\alpha_s \rho_s \sqrt{\theta\pi}} \right] \tag{23}$$

$$g_0 = \frac{1}{1 - \left(\frac{\alpha_s}{\alpha_{s,max}} \right)^{1/3}} \tag{24}$$

In particular, the KTGF solid viscosity and granular conductivity can be defined based on the following models:

Syamlal model (Syamlal et al., 1993)

$$\mu_{s,ktgf} = \frac{4}{5}\alpha_s^2 \rho_s d_p g_0(1 + e)\sqrt{\frac{\theta}{\pi}} + \frac{\alpha_s d_p \rho_s \sqrt{\pi\theta}}{6(3 - e)}\left[1 + \frac{2}{5}(1 + e)(3e - 1)\alpha_s g_0 \right] \tag{25}$$

$$\kappa_s = 2\alpha_s^2 \rho_s d_p g_0(1 + e)\sqrt{\frac{\theta}{\pi}} + \frac{9}{8}\sqrt{\theta\pi}\frac{\rho_s d_p g_0 \left(\frac{1}{2} + \frac{e}{2} \right)^2 (2e - 1)\alpha_s^2}{\left(\frac{49}{16} - \frac{33}{16}e \right)} + \frac{15}{32}\sqrt{\theta\pi}\frac{\alpha_s \rho_s d_p}{\left(\frac{49}{16} - \frac{33}{16}e \right)} \tag{26}$$

Gidaspow model (Gidaspow, 1994)

$$\mu_{s,\text{ktgf}} = \frac{4}{5}\alpha_s^2\rho_s d_p g_0(1+e)\sqrt{\frac{\theta}{\pi}}$$
$$+ \frac{2\frac{5\sqrt{\pi}}{96}\rho_s d_p\sqrt{\theta}}{(1+e)g_0}\left[1+\frac{4}{5}(1+e)\alpha_s g_0\right] \quad (27)$$

$$\kappa_s = 2\alpha_s^2\rho_s d_p g_0(1+e)\sqrt{\frac{\theta}{\pi}}$$
$$+ \frac{9}{8}\sqrt{\theta\pi}\rho_s d_p g_0\left(\frac{1}{2}+\frac{e}{2}\right)\alpha_s^2 \quad (28)$$
$$+ \frac{15}{16}\sqrt{\theta\pi}\alpha_s\rho_s d_p + \frac{25}{64}\sqrt{\theta\pi}\frac{\rho_s d_p}{(1+e)g_0}$$

Hrenya–Sinclair model (Hrenya and Sinclair, 1997)

$$\mu_{s,\text{ktgf}} = \frac{4}{5}\alpha_s^2\rho_s d_p g_0(1+e)\sqrt{\frac{\theta}{\pi}}$$
$$+ \frac{1}{15}\sqrt{\theta\pi}\frac{\rho_s d_p g_0(1+e)(\frac{3}{2}e-\frac{1}{2})\alpha_s^2}{(\frac{3}{2}-\frac{e}{2})}$$
$$+ \frac{1}{6}\sqrt{\theta\pi}\frac{\rho_s d_p\alpha_s\left(\frac{1}{2}\left(\frac{1+\lambda f_p}{R}\right)+\frac{3}{4}e-\frac{1}{4}\right)}{(\frac{3}{2}-\frac{e}{2})(1+\frac{\lambda f_p}{R})} \quad (29)$$
$$+ \frac{10}{96}\sqrt{\theta\pi}\frac{\rho_s d_p}{(1+e)g_0(\frac{3}{2}-\frac{e}{2})(1+\frac{\lambda f_p}{R})}$$

$$\kappa_s = 2\alpha_s^2\rho_s d_p g_0(1+e)\sqrt{\frac{\theta}{\pi}}$$
$$+ \frac{9}{8}\sqrt{\theta\pi}\frac{\rho_s d_p g_0\left(\frac{1}{2}+\frac{e}{2}\right)^2(2e-1)\alpha_s^2}{\left(\frac{49}{16}-\frac{33}{16}e\right)}$$
$$+ \frac{15}{16}\sqrt{\theta\pi}\frac{\alpha_s\rho_s d_p\left(\frac{\frac{e^2}{2}+\frac{1}{4}e+\frac{1}{4}+\lambda f_p}{R}\right)}{\left(\frac{49}{16}-\frac{33}{16}e\right)(1+\frac{\lambda f_p}{R})} \quad (30)$$
$$+ \frac{25}{64}\sqrt{\theta\pi}\frac{\rho_s d_p}{(1+e)\left(\frac{49}{16}-\frac{33}{16}e\right)(1+\frac{\lambda f_p}{R})g_0}$$

Figures 2 and 3 show the granular viscosity and granular conductivity as a function of the solid volume fraction, respectively. Both fields are computed for the same fluidization conditions of Figure 1, considering also a constant granular temperature of $\theta = 5 \times 10^{-4}\,\text{m}^2/\text{s}^2$ and a restitution coeficient of $e = 0.8$. All models predict similar values at high concentrations, but the Syamlal and Hrenya–Sinclair models have a sudden decrease in both granular parameters at very low concentrations. Regarding the granular conductivity, the Gidapsow model clearly predicts
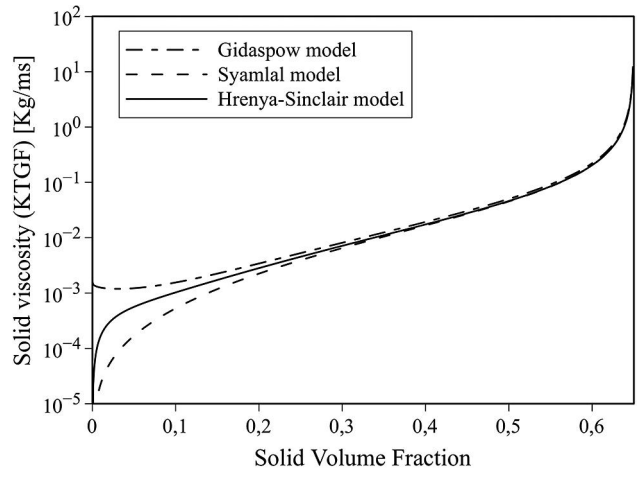

Figure 2. Solid viscosity $\mu_{s,\text{ktgf}}$ as function of the particles concentration for each model at bubbling fluidization conditions.

the higher values for the whole scope of particle concentrations.

Frictional particles interaction

At high concentrations, the particles are continuously in contact and the relative movement with each other produces rubbing and friction. In these conditions, the KTGF hypothesis (instantaneous and binary collisions) are not verified and another approach is needed to model the rheological parameters.

The first attempts to model this situation are based on treating the powder compound as a yielding plastic, where the frictional stress is given by the Coulomb law. In many cases, this condition
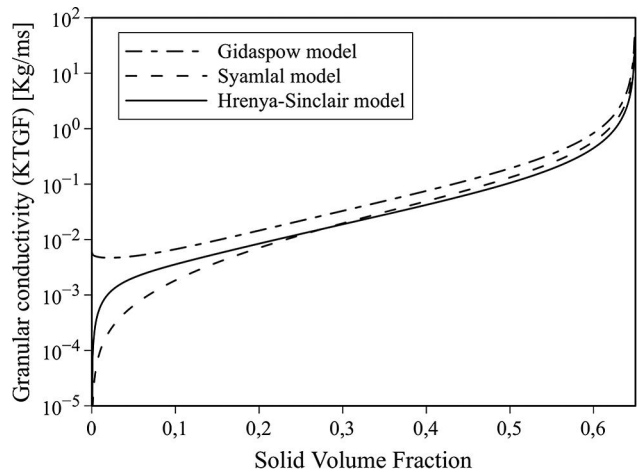

Figure 3. Granular conductivity $\kappa_{s,\text{ktgf}}$ as function of the particles concentration for each model at bubbling fluidization conditions.

is verified by the granular materials, where continuous deformation occur with no change on the volume (Tardos, 1997; Srivastava and Sundaresan, 2003). The following variants are commonly adopted (see Figure 4):

Model I

Johnson and Jackson (1987) proposed a model for the frictional normal stresses given by:

$$p_{s,\text{fric}} = Fr \frac{(\alpha_s - \alpha_{s,\min})^{\eta}}{(\alpha_{s,\max} - \alpha_s)^P} \qquad (31)$$

where $Fr = 0.05$, $\eta = 2$, and $P = 5$. Also, $\alpha_{s,min}$ is the minimal solid volume fraction at which frictional effects occur.

This model also considers that the frictional and collisional effects are additive. Therefore:

$$p_s = p_{s,\text{ktgf}} + p_{s,\text{fric}} \qquad (32)$$
$$\mu_s = \mu_{s,\text{ktgf}} + \mu_{s,\text{fric}} \qquad (33)$$

where $\mu_{s,fric}$ is considered to be proportional to the frictional pressure (according to the Coulomb law) and to the sine of the angle of internal friction:

$$\mu_{s,\text{fric}} = 0.5 \, p_{s,\text{fric}} \sin(\phi) \qquad (34)$$

Model II

Syamlal et al. (1993) proposed a model that isolate the contribution of both KTGF and frictional effects to the solids stress tensor:

$$(p_s, \mu_s) = \begin{cases} (p_{s,\text{ktgf}}, \mu_{s,\text{ktgf}}), & \text{if } \alpha_s < \alpha_{s,\min} \\ (p_{s,\text{fric}}, \mu_{s,\text{fric}}), & \text{if } \alpha_s \geq \alpha_{s,\min} \end{cases} \qquad (35)$$
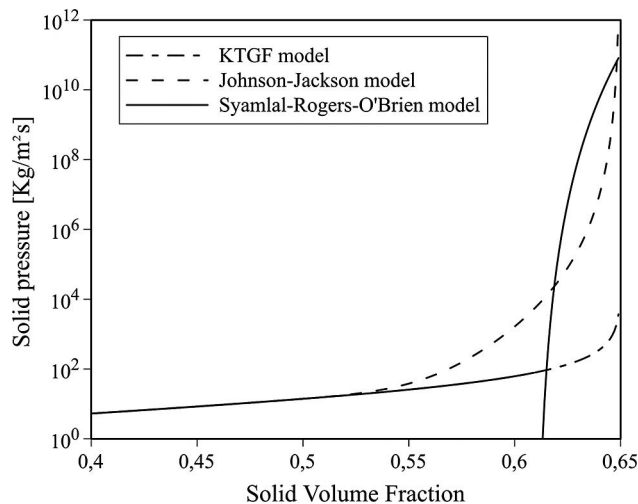

Figure 4. Frictional pressure $p_{s,fric}$ as function of the particles concentration for each model at bubbling fluidization conditions.

where the modeling of $\mu_{s,fric}$ is based on the work of Schaeffer (1987) who follows a more rigorous approach to establish the dissipative mechanism of granular flows. For this model, the frictional viscosity is defined as:

$$\mu_{s,\text{fric}} = 0.5 \, p_{s,\text{fric}} \, (I_{2D})^{-1/2} \, sin(\phi) \qquad (36)$$

where $(I_{2D})^{-1/2}$ is the second-order deviatoric shear stress tensor.

For this model, Syamlal et al. assumed an arbitrary function for the solid pressure to allow a certain degree compressibility given by:

$$p_{s,\text{fric}} = 10^{25}(\alpha_s - \alpha_{s,\min})^{10} \qquad (37)$$

Model III

This models makes use of the additive approach to define the rheological parameters, the Johnson and Jackson frictional model given by Eq. (31) and the model of Schaeffer for the solid viscosity given by Eq. (36).

Model IV

This model follows the work of Srivastava and Sundaresan (2003), which is similar to Model III but for the definition of the solid viscosity. The strain rate is modified according to the work of Savage (1998), who observed that shear stress in the granular assembly is lowered by the existence of fluctuations associated with the formation of shear layers even in quasi-static flow conditions, and that these layers length are around the same order of d_p. To contemplate this effect, an extra term is added to the shear stress modeling of Schaeffer Eq. (36) such that:

$$\mu_{s,\text{fric}} = 0.5 \, p_{s,\text{fric}} \left(I_{2D} + \frac{\theta}{d_p^2}\right)^{-1/2} sin(\phi) \qquad (38)$$

which is similar to the model adopted by Passalacqua and Marmo (2009). Here I_{2D} is the second invariant of the deviatoric rate strain tensor.

Three different approaches have been presented to compute the solid pressure. The first one corresponds to the KTGF model given by Lun et al. (1984) in Eq. (19) without considering frictional contributions. Another one is given by Eq. (37) with a switching approach Eq. (35) (Syamlal–Rogers–O'Brien model) between frictional and kinetic-collisional effects at certain solids

concentration (usually $\alpha_{s,min} = 0.61$). Finally, an additive approach given by Eq. (32) where both frictional and kinetic-collisional effects are simultaneously considered (Johnson–Jackson model) above certain concentration (see Eq. (31) with $\alpha_{s,min} = 0.5$). All these models are presented on Figure 4 as a function of the solids concentration, where it is observed that the isolated use of KTGF solid pressure leads to relative low normal stress predictions at high concentrations. At these conditions, the Johnson–Jackson pressure smoothly grows as the volume fraction is near the packing limit, at which the solids pressure becomes infinity. The Syamlal–Rogers–O'Brien model presents an expected discontinuous behavior due to the switching approach at $\alpha_{s,min}$, above which the solids pressure grows at a higher rate than the Johnson–Jackson model but, since it does not account for maximum packing, it ends up surpassed by the Johnson–Jackson pressure prediction near the maximum packing at $\alpha_s = 0.65$. This figure only refers to the solids normal stresses considered. In practice, it is used in conjunction with the solid shear stress model. Some selected combination of these models (as they usually appear in the literature) lead to the different alternatives presented in the previous paragraphs (Models I to IV).

Wall boundary conditions

In fluidized bed systems under the TFM technique, the correct adoption of boundary conditions at the walls for the solid phase is an open topic of discussion nowadays (Benyahia et al., 2005; Soleimani et al., 2015; Fede et al., 2016). Since the real nature of the granular phase is a set of individual particles, it is expected that the roughness of the wall affects the amount of sliding that the particulate phase experience in contact with the wall. Unlike a fluid phase, where a no-slip condition at the wall is naturally assumed, the wall boundary conditions for the granular phase may be more complex. One of the most popular approaches is to consider a mixed boundary condition for the solid phase velocity and granular temperature at the walls following the work of Johnson and Jackson (1987):

$$\frac{\partial \mathbf{u}_{s,w}}{\partial x} = \frac{\pi}{6} \frac{\alpha_{s,w}}{\alpha_{s,\max}} \varphi \rho_s g_0 \frac{\sqrt{3\theta_w}}{\mu_s} \mathbf{u}_{s,w} \qquad (39)$$

$$\frac{\partial \theta_w}{\partial x} = -\frac{\pi}{6} \frac{\alpha_{s,w}}{\alpha_{s,\max}} \varphi \frac{\rho_s^2}{\kappa_s} g_0 \frac{\sqrt{3\theta_w}}{\mu_s} |\mathbf{u}_{s,w}|^2$$
$$+ \frac{\pi}{4} \frac{\alpha_{s,w}}{\alpha_{s,\max}} (1 - e_w^2) \frac{\rho_s}{\kappa_s} g_0 \sqrt{3\theta_w^3} \qquad (40)$$

where φ is the specularity coefficient and e_w is the restitution coefficient between wall and particles. The specularity coefficient varies from 0, which corresponds to a smooth wall (fully slip condition), to 1 which correspond to a rough wall. In practice, this is a nonmeasurable parameter and it is usually specified through a data fitting of experimental results. In this context, Li and Benyahia (2012) proposed an expression for the specularity coefficient which consist of a function of other measurable parameters (frictional coefficient, slip velocity and wall restitution coefficient) generalizing its applicability to multiple flow conditions. The model uses the Johnson and Jackson formulas (Eqs. (39) and (40)), where the specularity is now defined as:

$$\varphi = \left(1 - \frac{d_p}{4|\mathbf{u}_{s,w}|} \frac{\partial |\mathbf{u}_{s,w}|}{\partial x}\right) \varphi' \qquad (41)$$

$$\varphi' = \begin{cases} -\frac{7\sqrt{6\pi}(\varphi_0')^2}{8k}, & \text{if } r \leq \frac{4k}{7\sqrt{6\pi}\varphi_0'} \\ \frac{2}{7}\frac{k}{r\sqrt{6\pi}}, & \text{otherwise} \end{cases} \qquad (42)$$

$$\varphi_0' = -0.0012596 + 0.1064551k - 0.04281476k^2$$
$$+ 0.0097594k^3 - 0.0012508258k^4$$
$$+ 0.0000836983k^5 - 0.00000226955k^6$$
$$(43)$$

$$r = \frac{|\mathbf{u}_{s,w}|}{\sqrt{3\theta}}, \quad k = \frac{7}{2}\mu(1 + e_w) \qquad (44)$$

where μ is the frictional coefficient between the particles material and the wall.

Another approach is presented by Schneider-bauer et al. (2012), which combines sliding and nonsliding conditions at the walls to derive the following expressions:

$$\frac{\partial \mathbf{u}_{s,w}}{\partial x} = N \mu \, \text{erf}\left(\sqrt{\frac{3}{2}}\frac{r}{\mu_0}\right) \qquad (45)$$

$$\frac{\partial \theta_w}{\partial x} = N\sqrt{3\theta} \left[\sqrt{\frac{2}{\pi}} \frac{\mu^2}{\mu_0^2} (1 + e_w - \mu_0) \exp\left(-\frac{3r^2}{2\mu_0^2}\right) r^2 \right.$$

$$+ \frac{\mu}{\sqrt{6\pi}\mu_0^2} (7\mu(1 + e_w) - 4\mu_0(1 + \mu)$$

$$- 3\mu\mu_0^2 (1 + e_w)) \exp\left(-\frac{3r^2}{2\mu_0^2}\right)$$

$$\left. + \frac{1}{\sqrt{6\pi}} (2(e_w - 1) + 3\mu^2(1 + e_2)) \right]$$

(46)

$$N = \sqrt{\frac{\pi}{24}} \frac{\rho_s \alpha_s g_0 (1 + e_w)\theta}{\alpha_{s,max}} \qquad (47)$$

$$\mu_0 = \frac{7}{2} \frac{(1 + e_w)}{(1 + \beta_0)} \mu \qquad (48)$$

where β_0 is the tangential restitution coefficient.

Numerical method

The presented model is solved using the finite volume method (Jasak, 1996; Ferziger and Peric, 2012). The coupling algorithm uses a combination of SIMPLE (Patankar and Spalding, 1972) and PISO (Issa, 1986) and it is fully implemented in the OpenFOAM® platform (Weller et al., 1998) based on the general structure of the `twoPhase-EulerFoam` solver (OpenFOAM® v2.2.0, April 2013. https://openfoam.org/release/2-2-0/) and the work of Passalacqua and Fox (2011). The coupling between phases is given through the partial elimination algorithm (Spalding, 1980; Oliveira and Issa, 2003) and a conservative formulation of the momentum equations is adopted. A detailed description of the code and its validation is found in the work of Venier et al. (2016)

Results

The drag, frictional and KTGF models previously presented are tested on two fluidized bed problems. The first test is based on an experiment performed by Kuipers et al. (1991) of a pseudo-2D bubbling fluidized bed with a central jet of gas at high speed. The interest here is to accurately predict the correct shape and detachment time of the first bubble. These results are known to be sensitive to the frictional model adopted (Passalacqua and Marmo, 2009), therefore various models will be tested and the results will be compared to the experimental results of the literature. For the second case, a

pseudo-2D bubbling fluidized bed is considered following the experimental setting of Laverman et al. (2008). For this problem, different drag models are explored along with different wall boundary conditions by analyzing time-averaged solid velocity profiles on a large time span. Unlike the previous problem, the transient states are not the main focus of interest. Instead, the solid particles distribution, velocity, and overall bed expansion is analyzed on a statistical steady state. The purpose of this section is to determine optimal modeling setups to accurately predict the overall hydrodynamics of pseudo-2D fluidized bed problems incorporating also the modeling criteria derived from the single bubble analysis of the first problem.

Bubbling fluidized bed with a central jet

This test is based on the experimental setup of Kuipers et al. (1991). The problem is schematized in Figure 5 and a simulation sequence of the bubble growth is shown in Figure 6. The modeling and numerical parameters are presented on Table 1. In particular, the drag coefficient is computed by the Gidaspow model. An estimation of the minimum fluidization velocity may be performed to determine if the model is applicable for the present problem conditions. This estimation is based on a
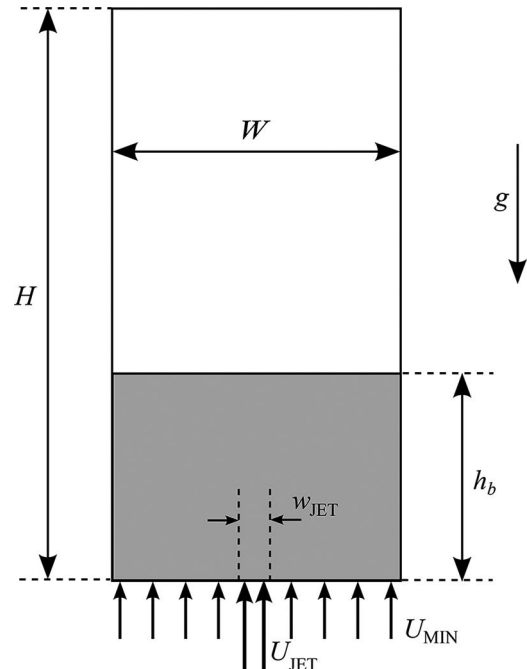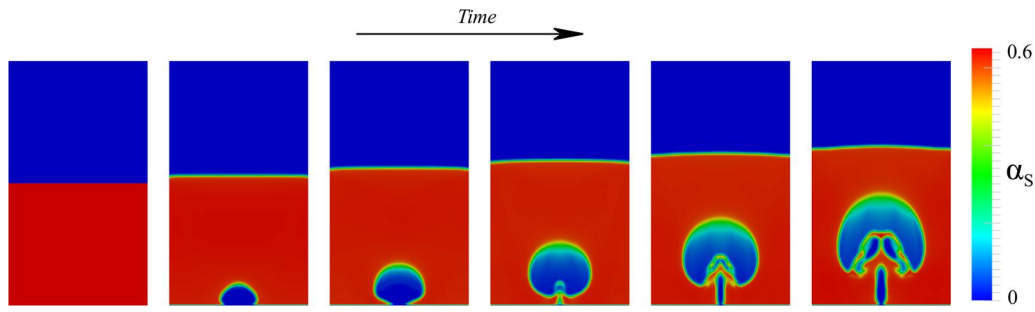

Figure 5. Single bubble rise scheme.

Time →

Figure 6. Bubble growth sequence.

balance between the buoyancy and the drag forces given by:

$$(\rho_s - \rho_g)\alpha_s^{mf}\alpha_g^{mf}g = K_{sg}u^{mf} \qquad (49)$$

where the superscript mf indicates the initial condition for the current field.

Thus, replacing Eq. (9) in Eq. (49), it yields that the minimum fluidization velocity for this problem is $u^{mf} \approx 0.22$ m/s which is 12% higher than the fluidization velocity reported experimentally by Kuipers et al. ($u_{exp}^{mf} \approx 0.25$ m/s). These differences are considered acceptable for the purpose of the present analysis which is mainly based on exploring the impact of different KTGF and frictional models on the bubble shape and detachment.

Figure 7 shows a comparison between experiment and simulation in terms of contour lines of time-averaged solid volume fraction after 40 seconds of physical time. There is a clear similitude on the overall particles distribution, with

slight differences near the walls and in the middle region. This may be attributed to a lack of averaging time in comparison to the experiment. Nevertheless, the performance of the solver is satisfactory in terms of bed expansion and overall particles distribution.

A mesh convergence analysis is performed to determine an optimal mesh size. Figures 8 and 9 show a single bubble growth at two different states of time for four different two-dimensional mesh refinements: 224 × 400 cells (1x), 112 × 200 cells (2x), 56 × 100 cells (4x), and 28 × 50 cells (8x). While all the refinements preserve the bubble shape, it is observed that the interphase for the 4x and 8x grids are highly diffusive. However, the 1x produce a slightly sharper interphase than the 2x grid, however the computational cost increase significantly. Therefore, the 2x mesh will be selected for further simulations.

Early works have shown differences between 2D and 3D simulations, which are mainly attributed to the effect of the front and back walls on the hydrodynamic behavior of pseudo-2D fluidized beds (Caicedo et al., 2002; Feng and Yu, 2010; Li et al., 2010a; Hernández-Jiménez et al., 2016). However, for the present problem conditions (i.e., inlet gas velocity, particles diameter, bed width, etc.) the 2D simulation produce a bubble shape similar to the 3D simulation, as presented in Figure 10. For the 3D simulation, 12 cells have been used to discretize the domain in the direction of the bed width, with a higher refinement near the front and back walls to capture the effect of the shear stress on the solids phase.

KTGF models

Figure 11 shows results for different solids viscosity and conductivity KTGF models (with no frictional modeling): Syamlal model (Eqs. (25) and (26)),

Table 1. Numerical parameters corresponding to Kuipers et al. experiment.

| Description	Value
Gas density	1.225 kg/m³
Gas viscosity	2.192×10^{-5} Pa s
Solid density	2660 kg/m³
Particles diameter	500 μm
Restitution coefficient	0.95
Width (W)	0.57 m
Height (H)	1 m
Bed initial height (h_b)	0.5 m
Jet inlet width (w_{JET})	0.015 m
Initial packing	0.598
Time step	1.0×10^{-5} s
Time discretization	Second-order implicit
Convective term scheme	Limited central difference
Number of PISO iterations	5
Number of outer iterations	10
Drag model	Gidaspow
Wall boundary condition	Johnson–Jackson
Fluidization velocity (U_{IN})	0.25 m/s
Jet inlet velocity (U_{JET})	10 m/s
Outlet pressure	0 Pa
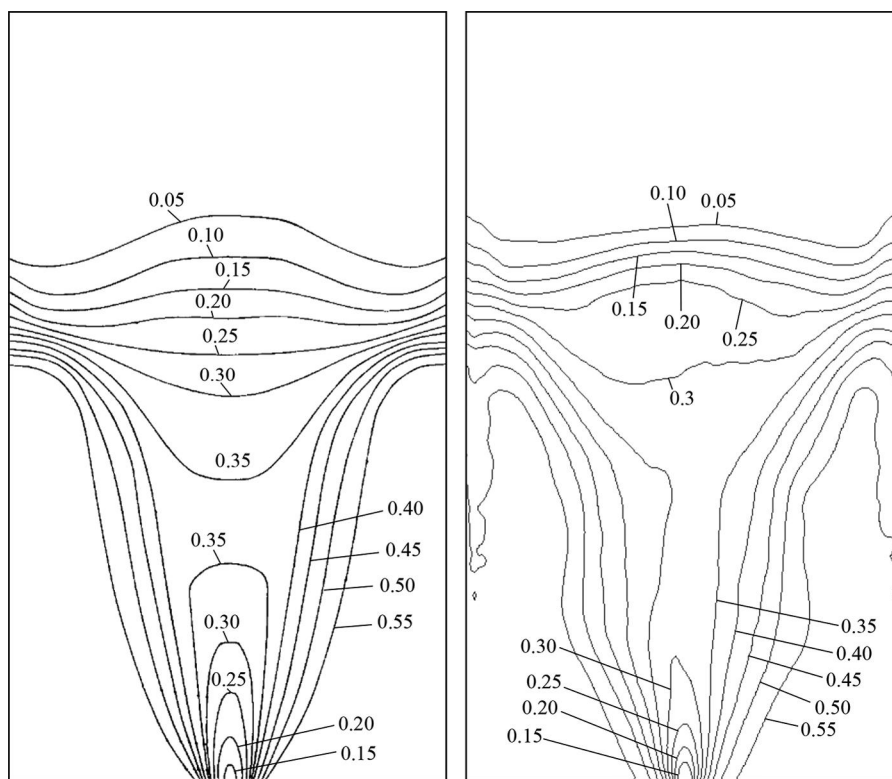
Figure 7. Time-averaged solid volume fraction contour lines: Experimental results from Kuipers et al. (left) and simulation results from this work (right).
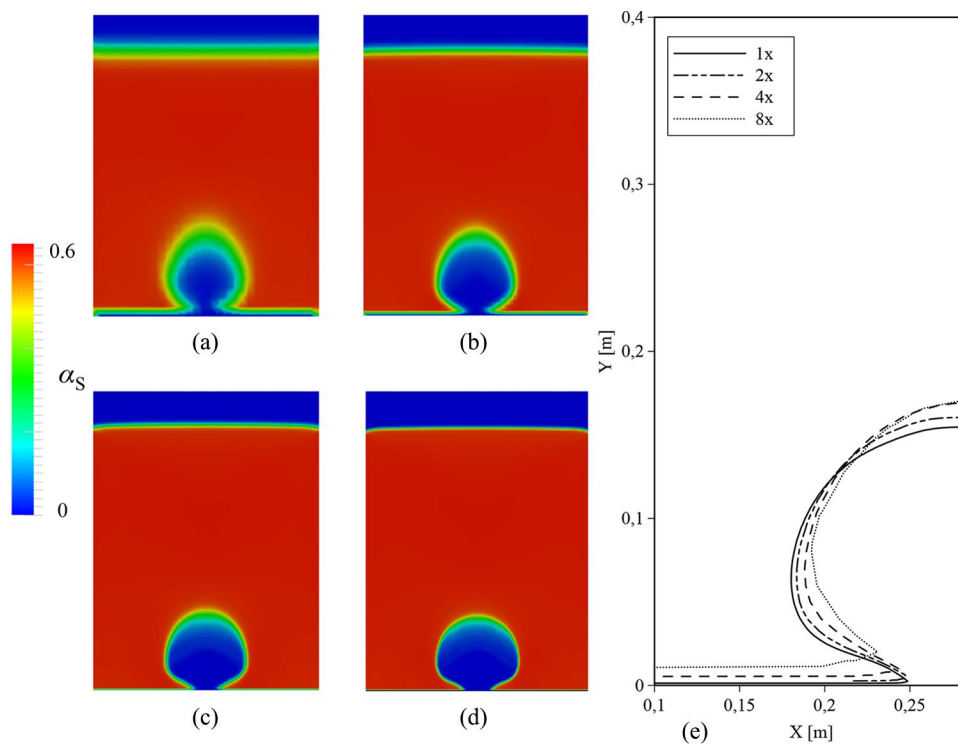

Figure 8. Bubble growth for different mesh sizes at t = 0.1s. (a) 8x, (b) 4x, (c) 2x, (d) 1x, and (e) contour lines for $\alpha_s = 0.2$.
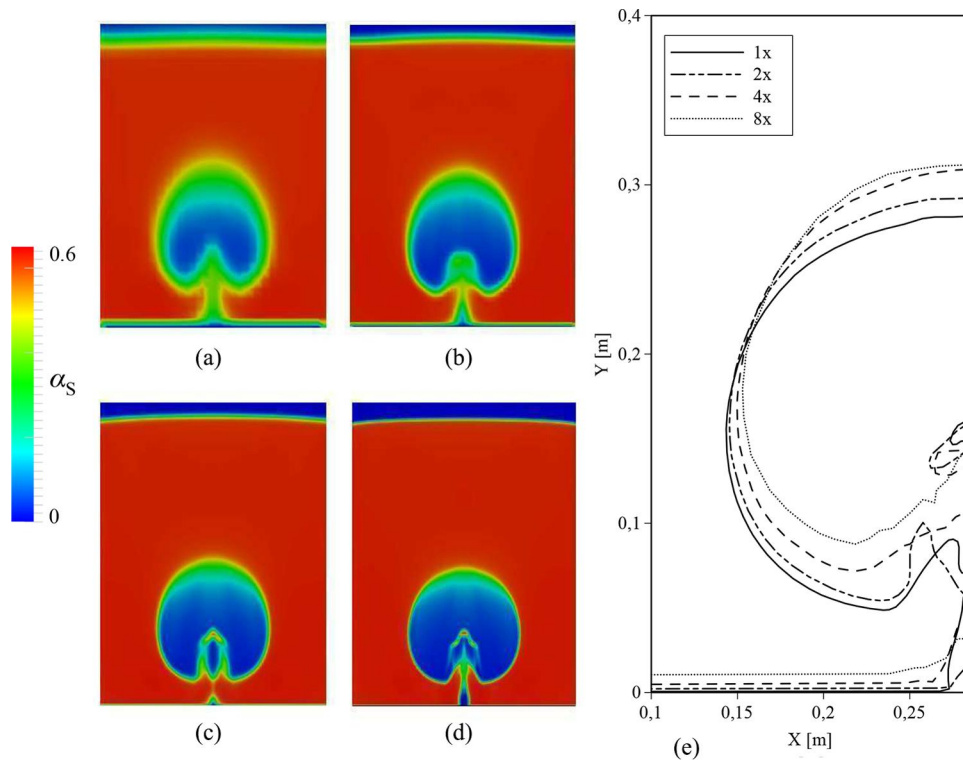
Figure 9. Bubble growth for different mesh sizes at $t = 0.2$s. (a) 8x, (b) 4x, (c) 2x, (d) 1x, and (e) contour lines for $\alpha_s = 0.2$.

Gidaspow model (Eqs. (27) and (28)), and Hrenya–Sinclair model (Eqs. (29) and (30)).

The results show that the shape of the bubble is not sensitive to the KTGF models adopted. This is expected since the bubble shape is mostly governed by the phase stress around the bubble, which is at near packing conditions. At such high concentrations, the different KTGF models tend to the same values of viscosity and granular conductivity. This agrees with the observations of Patil et al. (2005a) who states that the compaction around the bubble is not influenced by the particle-particle interaction due to collisional effects. However, when frictional effects are considered, the shape of the bubble
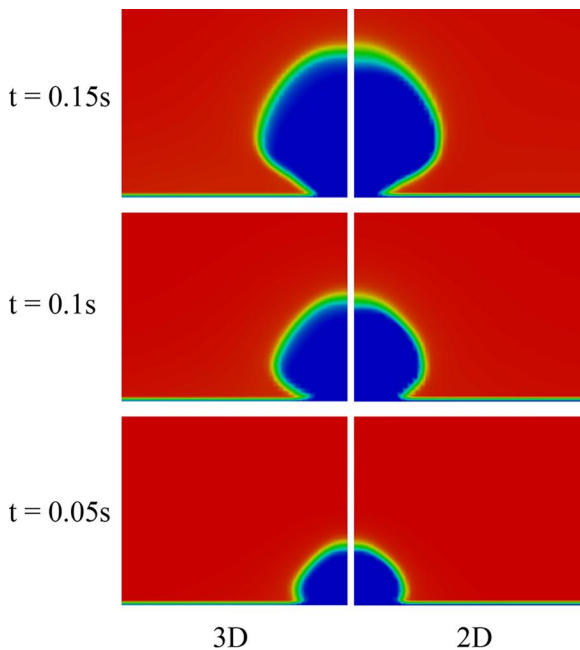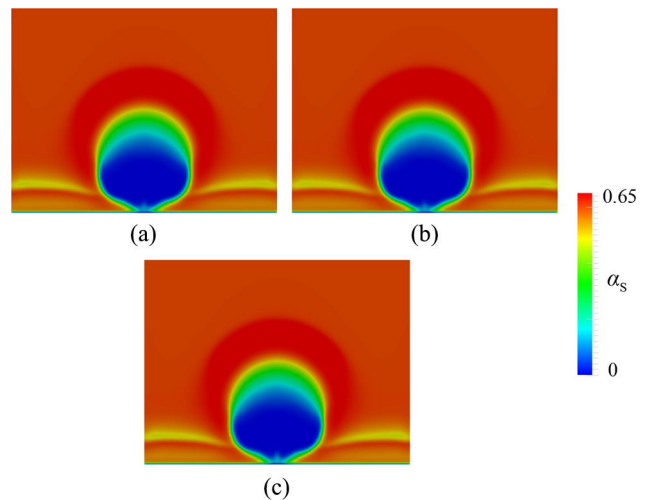

Figure 10. 2D and 3D simulations comparison.

Figure 11. Bubble at detachment time for different KTGF models: (a) Syamlal model, (b) Gidaspow model, and (c) Hrenya-Sinclair model.
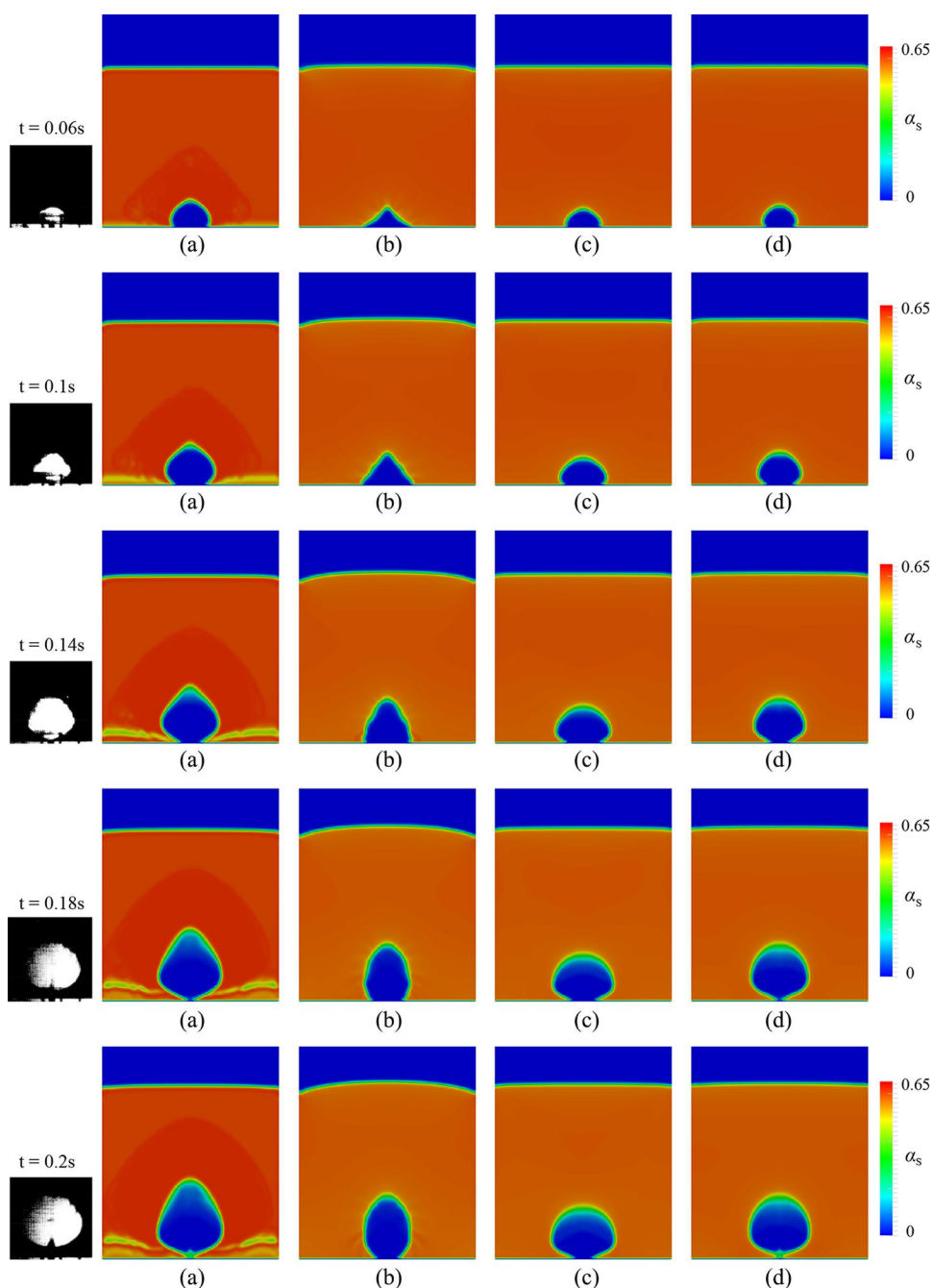
Figure 12. Bubble growth at different instants and frictional models: (a) Model I, (b) Model II, (c) Model III, and (d) Model IV.

becomes dependent of the stress model adopted (Patil et al., 2005a; Passalacqua and Marmo, 2009).

Frictional models

Figure 12 shows a qualitative comparison between four different frictional models along with experimental photographs at different states of time. It is clear that the Models I and II fails to predict the correct bubble shape, producing a more stretched and pointy bubble than the experiment. Models III and IV preserve the round shape of

the bubble, but Model III have a longer detachment time in comparison to the experiment (see Table 2). The same pattern is observed for Model IV but with a much closer agreement in terms of detachment time and bubble shape. Although there

Table 2. Bubble detachment time for different frictional models.

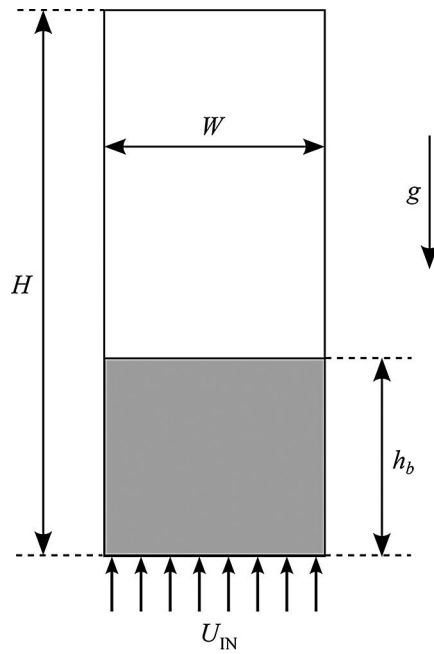| Experiment	Model I	Model II	Model III	Model IV
0.170 s	0.180 s	0.233 s	0.235 s	0.179 s

Figure 13. Bubbling fluidized bed scheme.

Table 3. Numerical parameters corresponding to Laverman et al. experiment.

Description	Value
Gas density	1.2 kg/m^3
Gas viscosity	2.2×10^{-5}Pa s
Solid density	2500 kg/m^3
Particles diameter	500 μm
Restitution coefficient	0.95
Width (W)	0.3 m
Height (H)	0.7 m
Bed initial height (h_b)	0.3 m
Initial packing	0.6
Time step	1.0×10^{-4} s
Time discretization	Second-order implicit
Convective term scheme	Limited central difference
Number of PISO iterations	5
Number of outer iterations	10
KTGF models	Syamlal
Frictional model	Model IV
Inlet velocity (U_{IN})	2.5 U$_f$
Minimal fluidization velocity (U_f)	0.18 m/s
Outlet pressure	0 Pa

are still some discrepancies in the time of detachment, this model clearly predicts the closest results to the experiment. This level of accuracy of the model may be attributed to the fact that, while the viscosity reaches very high values as the strain rate tends to zero for the Model III, the rheology given by Model IV becomes dependent of the granular temperature (Eq. (38)). This behavior have a more solid phenomenological foundation as presented by Savage (1998). The results also agrees with the observations of Passalacqua and Marmo (2009) for a bubbling fluidized bed with a central jet but under different experimental conditions.

Experiment of Laverman et al. (2008)

This test is based on the experimental setup of Laverman et al. (2008) and schematized in Figure 13. The modeling and numerical parameters are presented in Table 3. Figure 14 shows a sequence of simulation starting from a resting state using Syamlal–O'Brien model for the drag force and Syamlal model for the granular viscosity and conductivity and Model IV for the frictional effects.

A mesh convergence analysis is performed and the results of time-averaged vertical velocity at 0.3 m from the distributor are shown in Figure 15. It is clear that the 8x mesh overpredicts the amplitude of the velocity, while the 1x and 2x mesh results are in close agreement. Therefore, the 2x mesh is selected for the following simulations to minimize the computational requirements.

Figure 16 shows a comparison of results for 2D and a 3D simulations. Here, the time-averaged solid vertical velocity at $y = 0.3$ m and a vertical profile of time-averaged solid volume fraction are presented for both aproaches. The results show
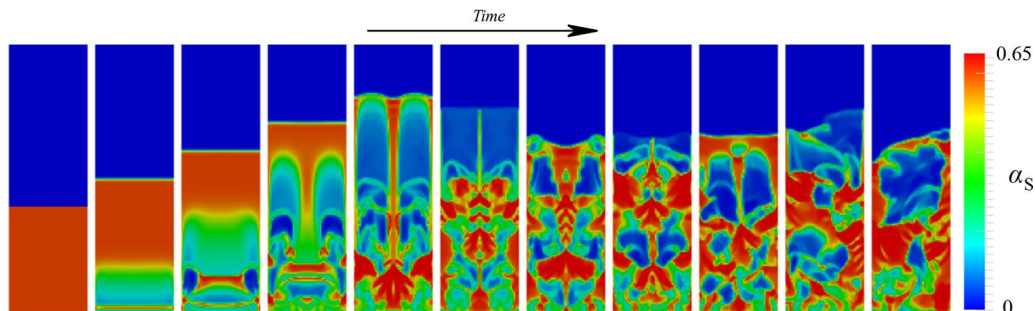

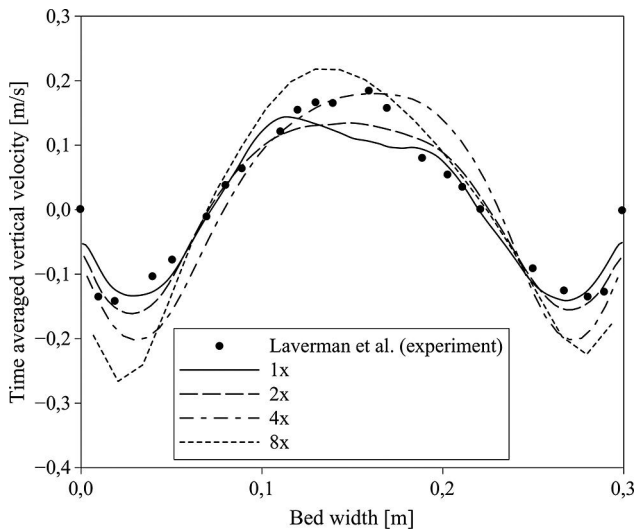**Figure 14.** Fluidization sequence.

Figure 15. Time-averaged vertical velocity profile for different mesh refinements at 0.3 m from the bottom.

strong similarities which suggest that the 2D simulations are addecuate enough for the present problem conditions (i.e., the front and back walls have a low impact on the hydrodynamics of the problem). These observation differ from the ones of Li et al. (2010a) for the same experiment, which may be attributed to the computational implementation of the TFM in both numerical codes (Syamlal et al., 1993; Weller et al., 1998).

Figure 17 shows two distinctive behaviors of the particulate phase from applying slip conditions (perfectly smooth wall where the particles in contact slide without resistance) and no-slip conditions (rough wall where particles cannot slide

in contact to the surface). The slip condition produce two counter-rotating vertical stretched vortices along the bed height with particles moving upward at high velocity in the middle zone and moving downward in contact to the walls. However, the no-slip condition presents two round vortices in the upper zone while the lower part is a zone presents a slow recirculating flow. Unlike the case with the slip condition, this behavior partially agrees with the experimental observation of Laverman et al. where a few difference may be appreciated near the walls where the particulate phase clearly continue its downward movement up to the bottom of the bed. Figure 18 shows the effect of considering different specularity coefficients by applying the Johnson-Jackson boundary conditions where it is clear that adopting slip or low values of the specularity coefficients lead to inaccurate results in terms of the time-averaged solid velocity fields.

Drag models

An estimation of the minimum fluidization velocity is performed for each of the drag models presented following the force balance given by Eq. (49). The results are presented on Table 4, where it is clear that the Syamlal–O'Brien model highly overpredicts the u^{mf}. This prohibits the use of the model for more detailed studies without a proper adjustment of the model parameters (Syamlal and O'Brien, 1987; Zimmermann and
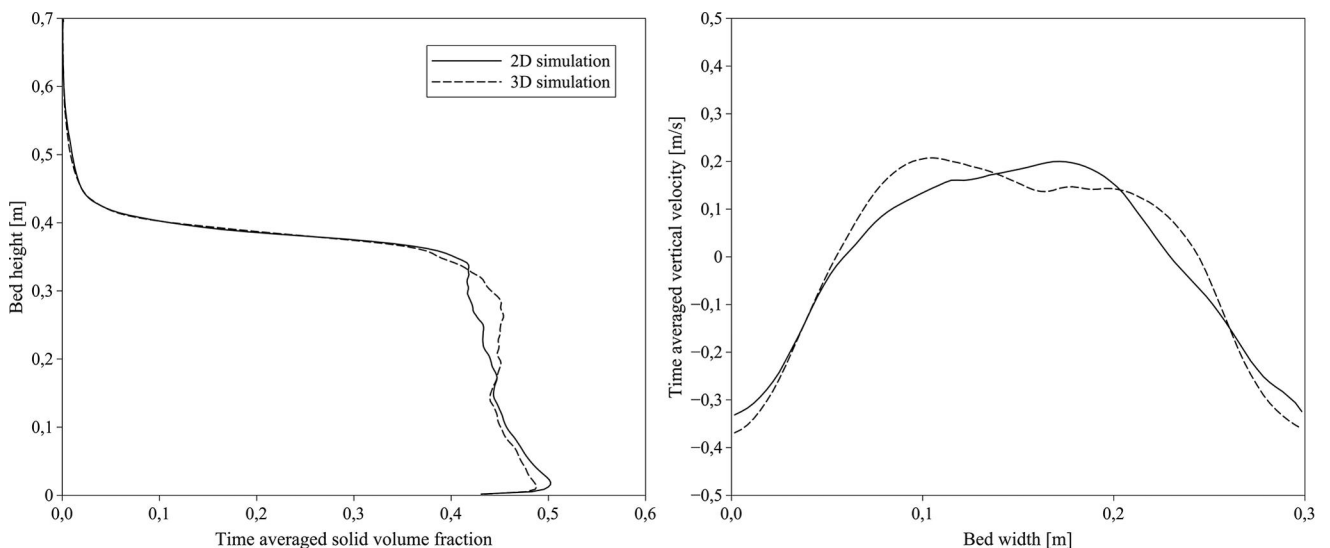

Figure 16. 2D vs 3D simulation comparison for the time averaged solid volume fraction on a vertical line (left) and time averaged solid vertical velocity at $y = 0.3$ m (right).
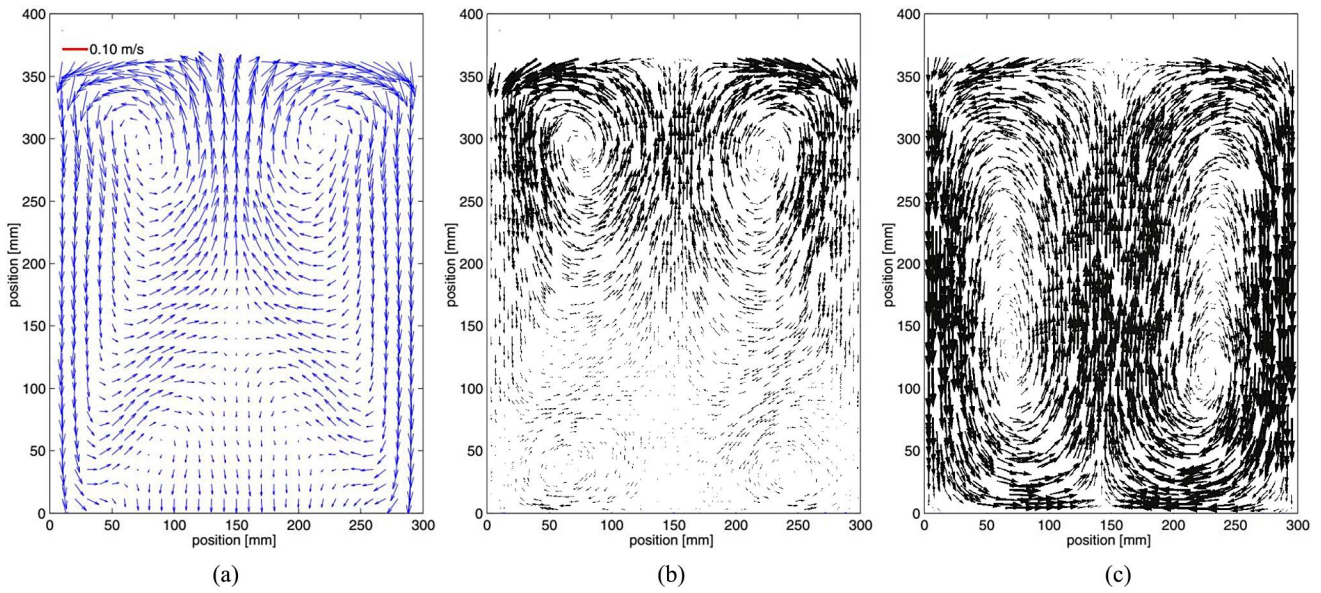
Figure 17. Solid phase velocity field vectors for (a) experiment, (b) no-slip condition, and (c) slip condition.
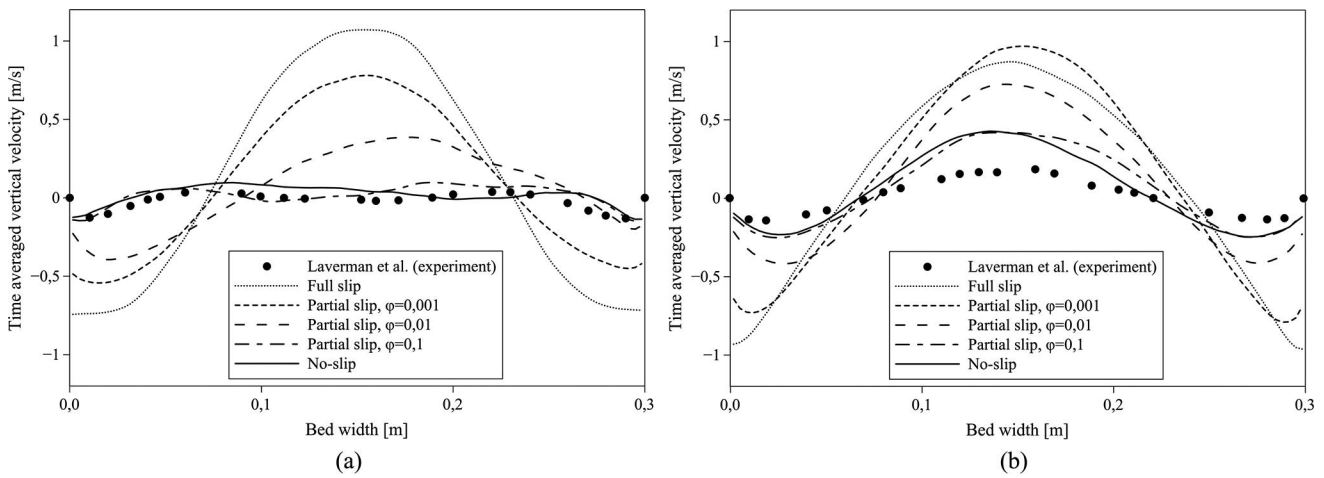

Figure 18. Time-averaged vertical velocity profile for different wall boundary conditions at (a) 0.1 m and (b) 0.3 m from the bottom.

Taghipour, 2005; Esmaili and Mahinpey, 2011). The same is extended to the Gibilaro model which fails to predict the u^{mf} with an error of ∼25%. The remaining models have a close agreement with the experimental results, with the small exception of the Di Felice model which will be adjusted in a similar manner as the Syamlal–O'Brien model. Since the nonadjusted Di Felice model is not far from the u_{mf} measured experimentally, it will also be considered in the following analysis.

For the Syamlal–O'Brien model, based on the experimental u_{mf}, the balance equation given by Eq. (49) may be solved along with a continuity condition for the coefficient B at $\alpha_g = 0.85$. This gives a new set of coefficients $C_1 = 11.183$ and $C_2 = 0.2$. However, the Di Felice model is adjusted through a slight modificiation of P and Q to produce the correct velocity of minimum fluidization ($P = 4$ and $Q = 0.582$).

Figure 19 shows time-averaged vertical solid velocity profile and volume fraction at 0.3 and

Table 4. Minimum fluidization velocity prediction for each drag model considered.

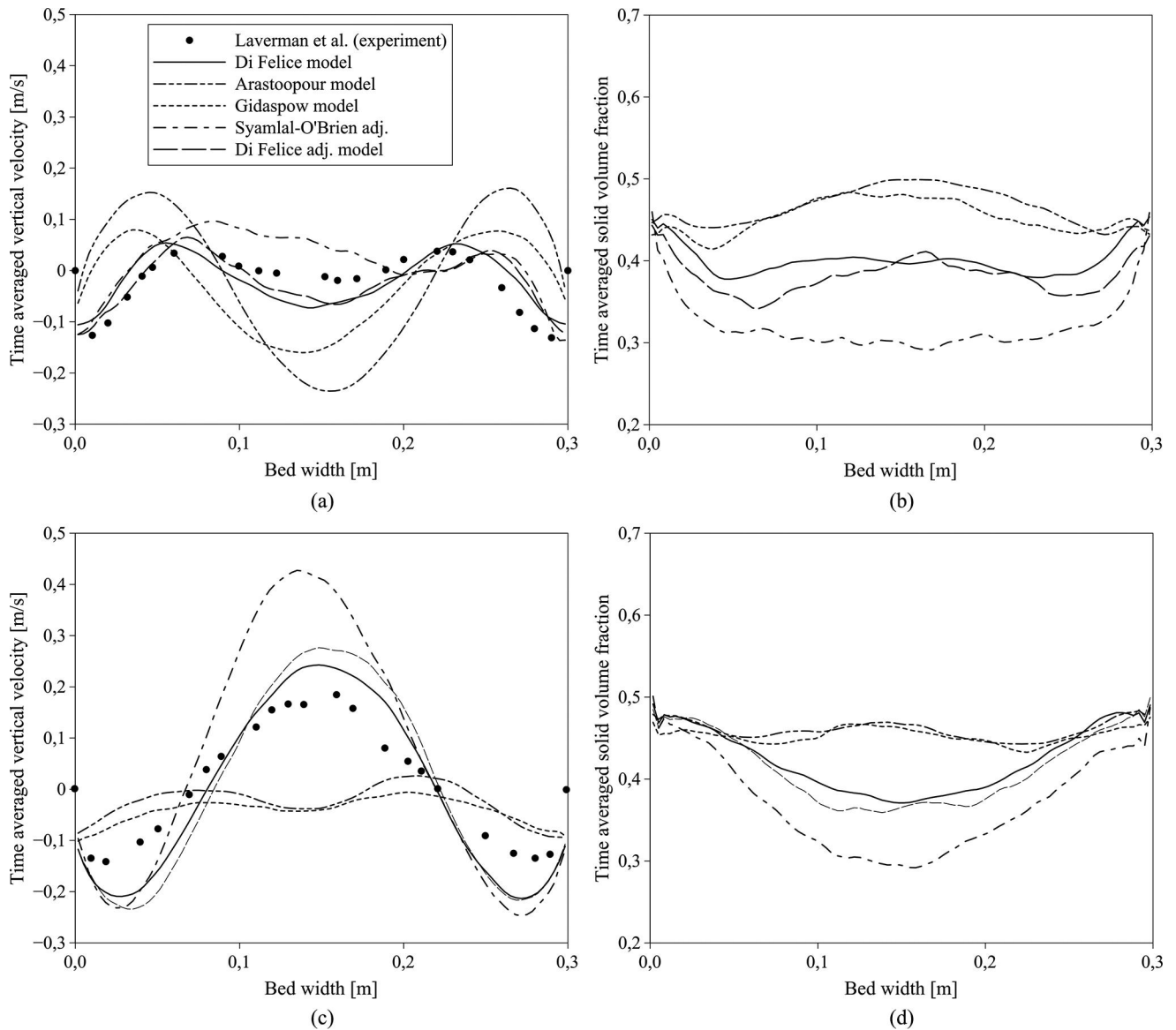| Drag models	Experiment	Gidaspow	Gibilaro	Syamlal–O'Brien	Arastoopour	Di Felice
u_{mf} (m/s)	0.18	0.1902	0.2411	0.6850	0.1901	0.2137

Figure 19. Time-averaged solid vertical velocity (a) and volume fraction (b) at 0.3 m, and solid vertical velocity (c) and volume fraction (d) at 0.1 m for different drag models.

0.1 m from the bottom. Figure 20 shows vertical time-averaged solid volume fraction and total pressure for different drag models. At 0.1 m from the distributor, some of the models tends to over-predict the maximum and minimum solids velocity (i.e., Gidaspow and Arastoopour models), while others, like the Di Felice model, accurately predicts the experimental results. This is emphasized at 0.3 m where the Di Felice model (both with and without the parameters adjustment) present a higher agreement with the experiment than the rest of the models. In fact, the Gidaspow and Arastoopour models tend to underpredict the maximum and minimum solids velocity, while the Syamlal–O'Brien (with the parameters

adjustment) tends to overpredict them. These differences are also observed on the bed expansion prediction (as depicted in Figure 20), where the Syamlal–O'Brien model produce the higher expansion. This behavior verifies the observations of Esmaili and Mahinpey (2011) and Vejahati et al. (2009), who showed that the Di Felice model produce very accurate results in terms of bed expansion, while the adjusted Syamlal–O'Brien produces an incorrect bed expansion which is clearly higher than the experimental predictions. In their work, they show that these differences increase as the inlet gas velocity becomes higher. This is observed in Figure 21 where solids velocity profiles at different gas inlet conditions are
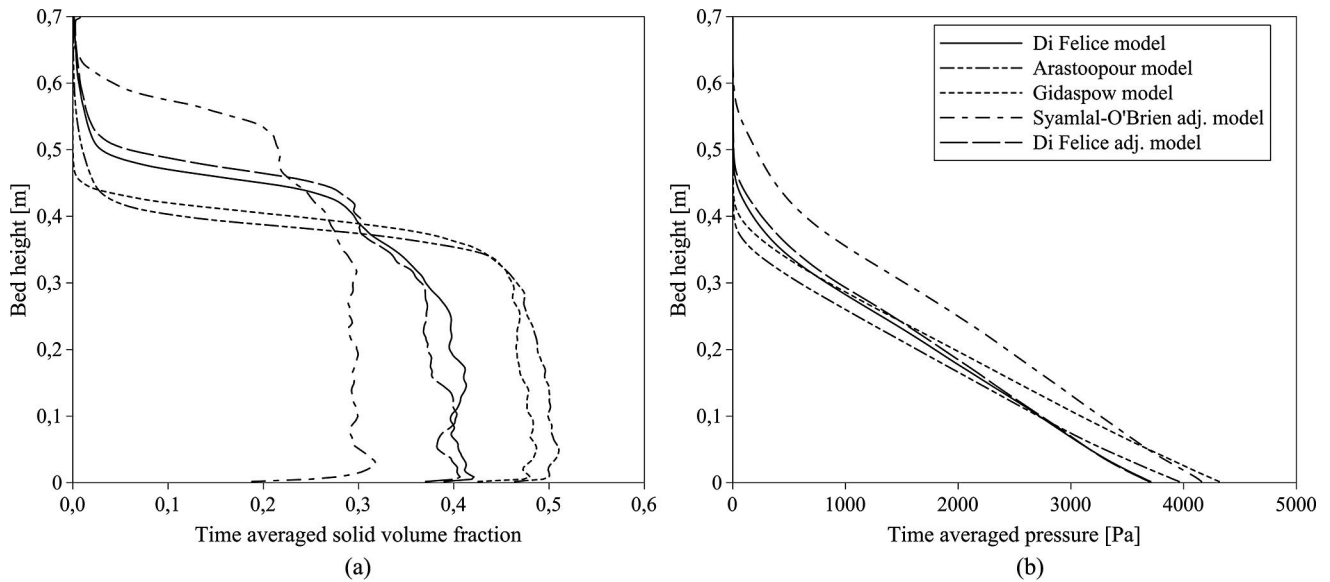
Figure 20. Time-averaged vertical profiles of volume fraction (a) and absolute pressure (b) for different drag models.

presented. Here, it is observed that both Di Felice models predict accurate velocity profiles while, in most cases, the Syamlal–O'Brien model overpredicts the solids velocity. Although the Di Felice models seems to be the most robust approach, it should be noticed that the velocity profile at the lower part of the bed with a gas velocity close to the minimum fluidization velocity cannot be captured with any of the drag models considered.

Wall boundary conditions

The selection of the correct wall boundary condition for the solid phase velocity for the multiple fluidization regimes is an open topic of discussion in the community (Benyahia et al., 2005; Li and Benyahia, 2012; Schneiderbauer et al., 2012; Fede et al., 2016). As was previously shown, the no-slip wall boundary conditions and the Johnson–Jackson conditions with a high specularity coefficient roughly predicts the general hydrodynamic behavior with good accuracy. In general, the Johnson–Jackson boundary conditions have more physical substance for addressing the behavior of the particles partially sliding against the walls. This model introduces the specularity coefficient which somehow indicates the roughness of the wall. As shown in the literature, the general flow behavior is highly sensitive to this parameter (Benyahia et al., 2005; Li et al., 2010a). Unfortunately, this is a nonmeasurable parameter which forces an apriori experimental practice to define

it for the particular problem conditions. Several authors proposed alternative methods which bypasses this issue (Jenkins and Louge, 1997; Li and Benyahia, 2012; Schneiderbauer et al., 2012). In this work, two of them (see Eqs. (41)–(44) and (45)–(48)) are tested along with the no-slip boundary conditions with the adjusted Di Felice drag model. A comparison in terms of the time-averaged solid velocity profile is presented on Figure 22. The results suggest that using the Li–Benyahia model (Li and Benyahia, 2012) is addecuate to estimate the correct specularity with a friction coefficient $\mu = 0.36$, predicting a velocity profile with the same agreement as the no-slip boundary conditions when compared to the experimental results. For the model proposed by Schneiderbauer et al., a tangential restitution $\beta_0 = 0$ and the same frictional coefficient as for the Li–Benyahia model are adopted. For these set of parameters and conditions, this model seems to overestimate the maximum and minimum solids velocity with respect to the other models. In all cases, a deeper analysis is needed to comprehend the discrepancies with the experimental results, specially in the region near the walls where the downward velocity is overestimated with all the models presented.

All the results of this work should be considered dependent of the computational code adopted (i.e., OpenFOAM®) and further validations need to be presented to ensure the capability of the code in

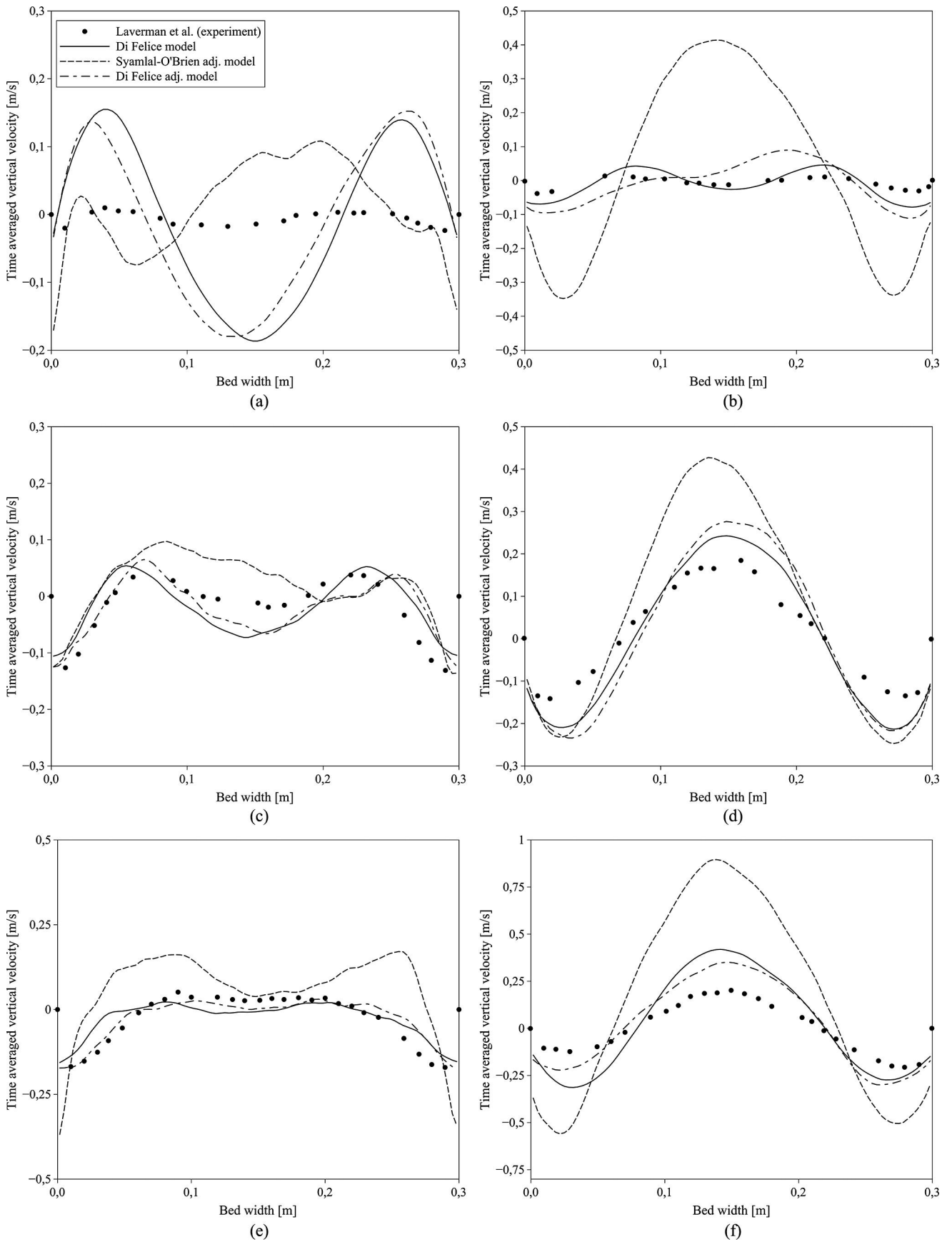**Figure 21.** Time-averaged solid vertical velocity for: (a) $U_{IN} = 1.5\,U_f$ at 0.1 m, (b) $U_{IN} = 1.5\,U_f$ at 0.3 m, (c) $U_{IN} = 2.5\,U_f$ at 0.1 m, (d) $U_{IN} = 2.5\,U_f$ at 0.3 m, (e) $U_{IN} = 3.5\,U_f$ at 0.1 m, (f) $U_{IN} = 3.5\,U_f$ at 0.3 m.
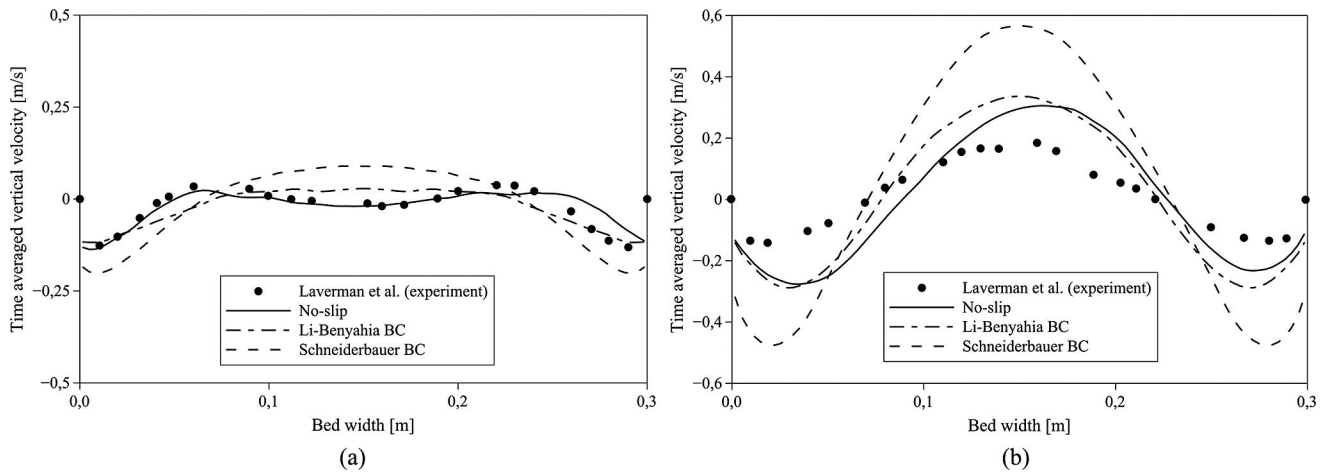
Figure 22. Time-averaged vertical velocity profile for different particle wall boundary conditions at (a) 0.1 m and (b) 0.3 m from the bottom with the adjusted Di Felice drag model.

predicting the correct solution for all possible fluidization regimes. In this aspect, Herzog et al. (2012) remarked some deficiencies in the code to produce the correct hydrodynamic behavior. However, in the last years, OpenFOAM® has proven to be a robust and efficient computational tool to address gas-particles systems (Passalacqua and Fox, 2011; Liu and Hinrichsen, 2014; Venier et al., 2016). This work intend to add another proof of accuracy of the code in this subject.

Conclusion

In this work, an open-source gas-particle flow solver was used to simulate two standard pseudo-2D bubbling fluidized bed problems. Different grid refinements were considered to determine an optimal mesh that balances the computational costs and the accuracy of the results for further studies.

Several modeling aspects with known sensitivity on the final results were analyzed. For the fluidized bed with a central jet problem, different KTGF and frictional models were tested. It was found that the adoption of different solid viscosity and granular conductivity models for the kinetic-collisional regime have a small impact on the results. This was expected since most of the evolution occurs at near-packing conditions. The bubble growth and detachment phenomenon is mostly dominated by the particulate phase compaction around the bubble where the solid stress is mostly dictated by the frictional models. In this sense, the higher agreement with the experimental results in terms

of bubble shape and time of detachment is given by the Model IV. This is somehow expected since it is the most physically contemplative out of the four models considered. For the uniformly fluidized bed problem, different boundary conditions for the solid phase and drag models were considered. Regarding the drag modeling, a preliminary study of the minimal fluidization velocity was performed. This was based on an approximated balance between buoyancy and drag forces which indicated that the Syamlal–O'Brien and the Gibilaro model should not be adopted without a parameters adjustment. Moreover, for different fluidization conditions, the Di Felice model with and without adjustment predicted the most accurate results in terms of time-averaged velocity profiles for the whole range of fluidization conditions. This may be attributed to the fact that this model is more contemplative, focusing on a data fitting function for the intermediate regimes which are largely influential in bubbling fluidization. Even when the models were successful to predict the velocities on the top of the bed, the results at the lower region, which are close to the minimum fluidization velocity, could not be fitted to experimental results at the same time. This implies that the drag models studied are still not able to cope all the bubbling fluidization regimes. Regarding the wall boundary conditions, the no-slip condition adoption for the particulate phase seems to be more adequate than the slip condition in bubbling regimes. A deeper analysis on granular-based wall boundary conditions was made by addressing three

different models. In this context, the Li and Benyahia model predicts accurate velocity profiles without incurring into further analysis to determine the specularity coefficient (as for the standard Johnson–Jackson conditions).

This analysis sought to provide more insight into the overall criteria for computational modeling of bubbling regimes on pseudo-2D fluidized bed. In most cases, a set of models with good agreement with the experimental results could be determined. However, it is the authors belief that, given the wide range of techniques and correlations to model the drag force, the frictional effects and the wall boundary conditions for different fluidization regimes, a preliminary modeling study to address new problem conditions cannot be avoided.

Funding

ORCID

Cesar M. Venier http://orcid.org/0000-0002-2139-6767

References

Arastoopour, H., Pakdel, P., and Adewumi, M. (1990). Hydrodynamic analysis of dilute gas–solids flow in a vertical pipe, *Powder Technol.*, **62**(2), 163–170.

Atkinson, J., and Bransby, P. (1977). The mechanics of soils, an introduction to critical state soil mechanics. Technical report.

Benyahia, S. (2008). Validation study of two continuum granular frictional flow theories, *Ind. Eng. Chem. Res.*, **47**(22), 8926–8932.

Benyahia, S., Syamlal, M., and O'Brien, T. J. (2005). Evaluation of boundary conditions used to model dilute, turbulent gas/solids flows in a pipe, *Powder Technol.*, **156**(2), 62–72.

Bouillard, J., Lyczkowski, R., and Gidaspow, D. (1989). Porosity distributions in a fluidized bed with an immersed obstacle, *AIChE J.*, **35**(6), 908–922.

Caicedo, G. R., Ruiz, M. G., Marqués, J. J. P., and Soler, J. G. (2002). Minimum fluidization velocities for gas–solid 2d beds, *Chem. Eng. Process. Process Intensif.*, **41**(9), 761–764.

Chapman, S., and Cowling, T. G. (1970). *The Mathematical Theory of Non-uniform Gases: An Account of the Kinetic Theory of Viscosity, Thermal Conduction and Diffusion in Gases*, Cambridge University Press, Cambridge CB2 8BS, United Kingdom.

Di Felice, R. (1994). The voidage function for fluid-particle interaction systems, *Int. J. Multiphase Flow*, **20**(1), 153–159.

Ding, J., and Gidaspow, D. (1990). A bubbling fluidization model using kinetic theory of granular flow, *AIChE J.*, **36**(4), 523–538.

Drew, D. A. (1982). Continuum modeling of two-phase flows. Technical report, DTIC Document.

Du, W., Bao, X., Xu, J., and Wei, W. (2006). Computational fluid dynamics (CFD) modeling of spouted bed: Assessment of drag coefficient correlations, *Chem. Eng. Sci.*, **61**(5), 1401–1420.

Enwald, H., Peirano, E., and Almstedt, A.-E. (1996). Eulerian two-phase flow theory applied to fluidization, *Int. J. Multiphase Flow*, **22**, 21–66.

Ergun, S. (1952). Fluid flow through packed columns, *Chem. Eng. Progress*, **48**, 89–94.

Esmaili, E., and Mahinpey, N. (2011). Adjustment of drag coefficient correlations in three dimensional CFD simulation of gas–solid bubbling fluidized bed, *Adv. Eng. Software*, **42**(6), 375–386.

Fede, P., Simonin, O., and Ingram, A. (2016). 3D numerical simulation of a lab-scale pressurized dense fluidized bed focussing on the effect of the particle-particle restitution coefficient and particle–wall boundary conditions, *Chem. Eng. Sci.*, **142**, 215–235.

Feng, Y., and Yu, A. (2010). Effect of bed thickness on the segregation behavior of particle mixtures in a gas fluidized bed, *Ind. Eng. Chem. Res.*, **49**(7), 3459–3468.

Ferziger, J. H., and Peric, M. (2012). *Computational methods for fluid dynamics*, Springer Science & Business Media.

Gibilaro, L., Di Felice, R., Waldram, S., and Foscolo, P. (1985). Generalized friction factor and drag coefficient correlations for fluid-particle interactions, *Chem. Eng. Sci.*, **40**(10), 1817–1823.

Gidaspow, D. (1994). *Multiphase Flow and Fluidization: Continuum and Kinetic Theory Descriptions*, Academic Press, California, USA.

Hernández-Jiménez, F., Sánchez-Prieto, J., Cano-Pleite, E., Garcia-Gutierrez, L., and Acosta-Iborra, A. (2016). Development of an empirical wall-friction model for 2d simulations of pseudo-2d bubbling fluidized beds, *Adv. Powder Technol.*, **27**(2), 521–530.

Herzog, N., Schreiber, M., Egbers, C., and Krautz, H. J. (2012). A comparative study of different cfd-codes for numerical simulation of gas–solid fluidized bed hydrodynamics, *Comput. Chem. Eng.*, **39**, 41–46.

Hrenya, C. M., and Sinclair, J. L. (1997). Effects of particle-phase turbulence in gas-solid flows, *AIChE J.*, **43**(4), 853–869.

Hui, K., Ungar, J., Haff, P., and Jackson, R. (1984). Boundary conditions for high-shear grain flows, *J. Fluid Mech.*, **145**(22), 233.

Ishii, M. (1975). Thermo-fluid dynamic theory of two-phase flow. NASA STI/Recon technical report A 75, 29657.

Issa, R. I. (1986). Solution of the implicitly discretised fluid flow equations by operator-splitting, *J. Comput. Phys.*, **62**(1), 40–65.

Jasak, H. (1996). Error analysis and estimation for the finite volume method with applications to fluid flows. Ph.D. thesis, Imperial College of Science, Technology and Medicine.

Jenkins, J., and Richman, M. (1986). Boundary conditions for plane flows of smooth, nearly elastic, circular disks, *J. Fluid Mech.*, **171**, 53–69.

Jenkins, J. T., and Louge, M. Y. (1997). On the flux of fluctuation energy in a collisional grain flow at a flat, frictional wall, *Phys. Fluids*, **9**(10), 2835–2840.

Johnson, P. C., and Jackson, R. (1987). Frictional–collisional constitutive relations for granular materials, with application to plane shearing, *J. Fluid Mech.*, **176**, 67–93.

Koksal, M., and Hamdullahpur, F. (2005). CFD simulation of the gas-solid flow in the riser of a circulating fluidized bed with secondary air injection, *Chem. Eng. Commun.*, **192**(9), 1151–1179.

Konan, N. A., Simonin, O., and Squires, K. (2006). Rough wall boundary condition derivation for particle continuum equations: Validation from LES/DPS of gas-solid turbulent channel flow. ASME 2006 2nd joint US-European fluids engineering summer meeting collocated with the 14th international conference on nuclear engineering, American Society of Mechanical Engineers, pp. 1723–1732.

Kuipers, J., Prins, W., and Van Swaaij, W. (1991). Theoretical and experimental bubble formation at a single orifice in a two-dimensional gas-fluidized bed, *Chem. Eng. Sci.*, **46**(11), 2881–2894.

Laverman, J. A., Roghair, I., Annaland, M. v. S., and Kuipers, H. (2008). Investigation into the hydrodynamics of gas–solid fluidized beds using particle image velocimetry coupled with digital image analysis, *Can. J. Chem. Eng.*, **86**(3), 523–535.

Li, T., and Benyahia, S. (2012). Revisiting Johnson and Jackson boundary conditions for granular flows, *AIChE J.*, **58**(7), 2058–2068.

Li, T., Grace, J., and Bi, X. (2010a). Study of wall boundary condition in numerical simulations of bubbling fluidized beds, *Powder Technol.*, **203**(3), 447–457.

Liu, Y., and Hinrichsen, O. (2014). CFD modeling of bubbling fluidized beds using OpenFOAM®: Model validation and comparison of TVD differencing schemes, *Comput. Chem. Eng.*, **69**, 75–88.

Loha, C., Chattopadhyay, H., and Chatterjee, P. K. (2012). Assessment of drag models in simulating bubbling fluidized bed hydrodynamics, *Chem. Eng. Sci.*, **75**, 400–407.

Lun, C., Savage, S., Jeffrey, D., and Chepurniy, N. (1984). Kinetic theories for granular flow: Inelastic particles in Couette flow and slightly inelastic particles in a general flowfield, *J. Fluid Mech.*, **140**, 223–256.

Lyczkowski, R. W., Gamwo, I. K., Dobran, F., Ai, Y., Chao, B., Chen, M., and Gidaspow, D. (1993). Validation of computed solids hydrodynamics and pressure oscillations in a bubbling atmospheric fluidized bed, *Powder Technol.*, **76**(1), 65–77.

Mazzei, L. (2008). Eulerian modelling and computational fluid dynamics simulation of mono and polydisperse fluidized suspension. Ph.D. thesis, UCL (University College London).

Oliveira, P. J., and Issa, R. I. (2003). Numerical aspects of an algorithm for the Eulerian simulation of two-phase flows, *International J. Numerical Methods in Fluids*, **43**(10–11), 1177–1198.

Parmentier, J.-F., Simonin, O., and Delsart, O. (2008). *A Numerical Study of Fluidization Behavior of Geldart B, A/B and A Particles Using an Eulerian Multifluid Modeling Approach*, Circulating Fluidized Bed Technology IX, Hamburg, Germany.

Passalacqua, A., and Fox, R. O. (2011). Implementation of an iterative solution procedure for multi-fluid gas–particle flow models on unstructured grids, *Powder Technol.*, **213**(1), 174–187.

Passalacqua, A., and Marmo, L. (2009). A critical comparison of frictional stress models applied to the simulation of bubbling fluidized beds, *Chem. Eng. Sci.*, **64**(12), 2795–2806.

Patankar, S. V., and Spalding, D. B. (1972). A calculation procedure for heat, mass and momentum transfer in three-dimensional parabolic flows, *Int. J. Heat Mass Transfer*, **15**(10), 1787–1806.

Patil, D., van Sint Annaland, M., and Kuipers, J. (2005a). Critical comparison of hydrodynamic models for gas–solid fluidized beds - Part I: Bubbling gas–solid fluidized beds operated with a jet, *Chem. Eng. Sci.*, **60**(1), 57–72.

Patil, D., van Sint Annaland, M., and Kuipers, J. (2005b). Critical comparison of hydrodynamic models for gas–solid fluidized beds - Part II: Freely bubbling gas–solid fluidized beds, *Chem. Eng. Sci.*, **60**(1), 73–84.

Richardson, J., and Zaki, W. (1954). The sedimentation of a suspension of uniform spheres under conditions of viscous flow, *Chem. Eng. Sci.*, **3**(2), 65–73.

Savage, S. (1998). Analyses of slow high-concentration flows of granular materials, *J. Fluid Mech.*, **377**, 1–26.

Schaeffer, D. G. (1987). Instability in the evolution equations describing incompressible granular flow, *J. Diff. Equat.*, **66**(1), 19–50.

Schneiderbauer, S., Schellander, D., Löderer, A., and Pirker, S. (2012). Non-steady state boundary conditions for collisional granular flows at flat frictional moving walls, *Int. J. Multiphase Flow*, **43**, 149–156.

Sinclair, J., and Jackson, R. (1989). Gas-particle flow in a vertical pipe with particle-particle interactions, *AIChE J.*, **35**(9), 1473–1486.

Soleimani, A., Schneiderbauer, S., and Pirker, S. (2015). A comparison for different wall-boundary conditions for kinetic theory based two-fluid models, *Int. J. Multiphase Flow*, **71**, 94–97.

Spalding, D. (1980). Numerical computation of multi-phase fluid flow and heat transfer, *Recent Adv. Numer. Methods Fluids*, **1**, 139–167.

Srivastava, A., and Sundaresan, S. (2003). Analysis of a frictional–kinetic model for gas–particle flow, *Powder Technol.*, **129**(1), 72–85.

Syamlal, M. (1987). The particle-particle drag term in a multiparticle model of fluidization. Tech. rep., EG and G Washington Analytical Services Center, Inc., Morgantown, WV, USA.

Syamlal, M., and O'Brien, T. (1987). The derivation of a drag coefficient formula from velocity-voidage correlations. Technical Note, US Department of energy, Office of Fossil Energy, NETL, Morgantown, WV.

Syamlal, M., Rogers, W., and OBrien, T. J. (1993). MFIX documentation: Theory guide. National Energy Technology Laboratory, Department of Energy, Technical Note DOE/METC-95/1013 and NTIS/DE95000031.

Taghipour, F., Ellis, N., and Wong, C. (2005). Experimental and computational study of gas–solid fluidized bed hydrodynamics, *Chem. Eng. Sci.*, **60**(24), 6857–6867.

Tardos, G. I. (1997). A fluid mechanistic approach to slow, frictional flow of powders, *Powder Technol.*, **92**(1), 61–74.

Vejahati, F., Mahinpey, N., Ellis, N., and Nikoo, M. B. (2009). Cfd simulation of gas–solid bubbling fluidized bed: A new method for adjusting drag law, *Can. J. Chem. Eng.*, **87**(1), 19–30.

Venier, C. M., Damian, S. M., and Nigro, N. M. (2016). Numerical aspects of Eulerian gas–particles flow formulations, *Comput. Fluids*, **133**, 151–169.

Wang, H., Yang, W., Senior, P., Raghavan, R., and Duncan, S. (2008). Investigation of batch fluidized-bed drying by mathematical modeling, CFD simulation and ECT measurement, *AIChE J.*, **54**(2), 427–444.

Weller, H. G., Tabor, G., Jasak, H., and Fureby, C. (1998). A tensorial approach to computational continuum mechanics using object-oriented techniques, *Comput. Phys.*, **12**(6), 620–631.

Wen, C., and Yu, Y. (1966). Mechanics of fluidization, *Chem. Eng. Progress Symp.*, **62**, 100–111.

Yuu, S., Nishikawa, H., and Umekage, T. (2001). Numerical simulation of air and particle motions in group-B particle turbulent fluidized bed, *Powder Technology*, **118**(1), 32–44.

Zimmermann, S., and Taghipour, F. (2005). Cfd modeling of the hydrodynamics and reaction kinetics of fcc fluidized-bed reactors, *Ind. Eng. Chem. Res.*, **44**(26), 9818–9827.